# Construction of a Ground-Motion Logic Tree through Host-to-Target Region Adjustments Applied to an Adaptable Ground-Motion Prediction Model

David M. Boore[*1], Robert R. Youngs[2], Albert R. Kottke[3], Julian J. Bommer[4], Robert Darragh[5], Walter J. Silva[5], Peter J. Stafford[4], Linda Al Atik[6], Adrian Rodriguez-Marek[7], and James Kaklamanos[8]

## ABSTRACT

**The purpose of a median ground-motion logic tree is to capture the center, body, and range of possible ground-motion amplitudes for each earthquake scenario considered in a seismic hazard analysis. For site-specific hazard analyses, the traditional approach of populating the logic tree branches with ground-motion prediction models (GMPMs) selected and weighted on the basis of vaguely defined applicability to the target region is rapidly being abandoned in favor of the backbone GMPM approach. In this approach, the selected backbone model is first adjusted to match the earthquake source and path characteristics of the target region, and then it is separately adjusted to account for the site-specific geotechnical profile. For a GMPM to be amenable to such host-to-target adjustments, the magnitude scaling of response spectral ordinates should be consistent with the theoretical scaling of Fourier amplitude spectra. In addition, the influence of individual source and path parameters should be clearly distinguished in the model to allow the adjustments to be applied individually, and reliable estimates of the source and path parameters from the host region of the GMPM should be available, as should a reference rock profile for the model. The NGA-West2 project GMPM of Chiou and Youngs (2014; hereafter, CY14) has been identified as a very suitable backbone model. Moreover, rather than adopting generic source and path parameters and a rock site profile from the host region for CY14, which is not easily defined because the data from which it was derived came from several geographical locations, recent studies have inverted the model to obtain a CY14-consistent reference rock profile and CY14-compatible source and path parameters. Using these host-region characteristics, this study illustrates the process of building a ground-motion logic tree through the sequential application of multiple host-to-target-region adjustments, each represented by a node on the logic tree to achieve a tractable model for the total epistemic uncertainty.**

## KEY POINTS

- A procedure is given to adjust a ground-motion model for use in seismic hazard analysis in a target region.
- We provide a step-by-step procedure for the host-to-target-region adjustment stated in key point 1.
- The suggested procedures should be useful for probabilistic seismic hazard calculations in any region.

**Supplemental Material**

1. Consultant, Los Altos, California, U.S.A., https://orcid.org/0000-0002-8605-9673 (DMB); 2. Wood Environment & Infrastructure Solutions, Inc., Oakland, California, U.S.A., https://orcid.org/0000-0002-1992-046X (RRY); 3. Pacific Gas & Electric Company, San Francisco, California, U.S.A., https://orcid.org/0000-0002-1861-5682 (ARK); 4. Department of Civil and Environmental Engineering, Imperial College London, London, United Kingdom, https://orcid.org/0000-0002-9709-5223 (JJB); https://orcid.org/0000-0003-0988-8934 (PJS); 5. Pacific Engineering & Analysis, El Cerrito, California, U.S.A.; 6. Al Atik Consulting, San Francisco, California, U.S.A., https://orcid.org/0000-0002-2979-8330 (LAA); 7. Department of Civil and Environmental Engineering, Virginia Tech, Blacksburg, Virginia, U.S.A., https://orcid.org/0000-0002-8384-4721 (AR-M); 8. Department of Civil Engineering, Merrimack College, North Andover, Massachusetts, U.S.A., https://orcid.org/0000-0001-7480-0391 (JK)

*Corresponding author: dboore@yahoo.com

**Cite this article as** Boore, D. M., R. R. Youngs, A. R. Kottke, J. J. Bommer, R. Darragh, W. J. Silva, P. J. Stafford, L. Al Atik, A. Rodriguez-Marek, and J. Kaklamanos (2022). Construction of a Ground-Motion Logic Tree through Host-to-Target Region Adjustments Applied to an Adaptable Ground-Motion Prediction Model, *Bull. Seismol. Soc. Am.* **112**, 3063–3080, doi: 10.1785/0120220056

## INTRODUCTION

Logic trees are used ubiquitously in probabilistic seismic hazard analysis (PSHA) to incorporate epistemic uncertainty in each of the elements of the models characterizing seismic sources and ground motions. The fundamental objective of logic trees is to capture the center, the body, and the range (CBR) of technically defensible interpretations (TDI) of the available data, methods, and models (U.S. Nuclear Regulatory Commission [USNRC], 2018). For ground-motion characterization (GMC) models, this translates into defining, for each earthquake scenario specified by the seismic source characterization model, the full distribution of possible ground-motion amplitudes. Constructing GMC logic trees by populating the branches with published ground-motion prediction models (GMPMs), selected on the basis of their applicability—inferred or tested using local data, often from small-magnitude earthquakes—is unlikely to capture the CBR of TDI. Even in regions with abundant ground-motion data, the published GMPMs are not considered to adequately capture the full range of epistemic uncertainty (e.g., Al Atik and Youngs, 2014), and it is very unlikely that the published GMPMs will capture the range when applied to the target region. Moreover, there is a fundamental problem in the traditional approach of populating the logic-tree branches with published GMPMs, namely that the relationship between the weights on the models and the weights on the resulting distributions of ground-motion amplitudes is opaque. All of these considerations have given rise to alternative techniques, collectively called the "backbone GMPM" approach (Bommer, 2012), in which the branches of the GMC logic tree are populated by scaled versions of a single-backbone GMPM (e.g., Atkinson *et al.*, 2014). A key part of the backbone GMPM approach is that weights are assigned to logic-tree branches to reflect the relative degree of confidence in each alternative model or parameter value; these weights are subsequently treated as probabilities in the calculation of the mean hazard and the associated fractiles. This requires the alternative branches at each node to satisfy the MECE (mutually exclusive and collectively exhaustive) criterion (e.g., Bommer and Scherbaum, 2008), which is unlikely to be the case using multiple GMPMs derived from overlapping datasets, whereas the logic-tree branches will inevitably be mutually exclusive using the backbone approach.

Using only published GMPMs from a different (host) region will seldom capture the center of the distribution, because the host and target regions are rarely, if ever, perfect analogs. Moreover, published GMPMs with generic site amplification factors conditioned on parameters such as $V_{S30}$ (time-averaged shear-wave velocity in the upper 30 m of the subsurface) and $Z_{1.0}$ or $Z_{2.5}$ (depths to shear-wave velocity horizons of 1.0 km/s and 2.5 km/s, respectively) are very unlikely to capture the dynamic response characteristics of the target site. For these reasons, the development of a site-specific GMC logic-tree will generally require host-to-target adjustments to render each GMPM more applicable to the target region and site. Within the backbone framework, the adjustments for differences in source, path, and site characteristics between the host region of the GMPM and the target region and site of the PSHA provides a tractable way to develop the distribution of epistemic uncertainty by assigning branches for the uncertainty in the estimates of each variable for which the adjustments are made.

When a GMC logic tree is to be constructed by applying a series of host-to-target adjustments to a backbone GMPM, the emphasis in selecting the backbone model shifts from seeking a model that is in some sense applicable to the target region to identifying a model that is amenable to being adjusted to match the target-region characteristics. An adaptable GMPM can be broadly defined as one in which the influence of each individual source and path parameter is clearly identifiable and isolated, and in which the scaling of response spectral accelerations with magnitude is consistent with the theoretical scaling based on Fourier amplitude spectra (FAS) in stochastic simulations (Boore, 2003). Bommer and Stafford (2020) identified the NGA-West2 project model of Chiou and Youngs (2014; hereafter, CY14) as the most adaptable GMPM for shallow crustal seismicity, because its formulation is the most consistent with seismological theory.

To apply the host-to-target adjustments, estimates are needed for the source, path, and site parameters of the host region where the backbone GMPM was developed, and for the target region and site for which the PSHA is being conducted. When applying such hybrid empirical adjustments, it has been a common practice to compile host-region parameters from seismological studies conducted in the region represented by the backbone GMPM (e.g., Campbell, 2003). A preferable approach, especially for models such as the NGA-West2 GMPMs that are derived from a dataset compiled from several active crustal regions, is to determine a suite of source, path, and site parameters that collectively optimize the match of the output from stochastic simulations with the predictions from the GMPM over the ranges of magnitude and distance of the greatest relevance to the PSHA calculations (e.g., Scherbaum *et al.*, 2006). Using the host crustal shear-wave velocity ($V_S$) profile and high-frequency attenuation (kappa) value determined for the CY14 GMPM by Al Atik and Abrahamson (2021), Stafford *et al.* (2022) have determined a suite of source and path parameters for the effective host region of the CY14 GMPM, which provide the starting point for any application using this model as a backbone GMPM.

The purpose of this article is to illustrate the process of applying multiple host-to-target adjustments to the CY14 backbone GMPM to construct a GMC logic tree for PSHA. The target location is the Idaho National Laboratory (INL), where a Senior Seismic Hazard Analysis Committee

(SSHAC) Level 3 PSHA (Ake *et al.*, 2018) is currently underway. The adjustments are illustrated only for source and path parameters, consistent with the development of the GMC model for PSHA, which is incorporating site response effects using the convolution approach of Bazzurro and Cornell (2004), usually referred to as approach 3 (McGuire *et al.*, 2001). Traditionally, this approach has involved adjusting the GMPMs to a buried reference rock horizon and then convolving the hazard at this horizon with the amplification factors for the overlying layers, effectively applying the site adjustment in two steps (e.g., Rodriguez-Marek *et al.*, 2014). In the INL PSHA project, in common with other recent projects, the hazard calculations are conducted using the source- and path-adjusted backbone GMPM but retaining the host reference rock profile. The site adjustments are then applied in a single step, using the ratio of the amplification factors for the full crustal profiles for the target site to those for the host reference rock profile anchored to a $V_{S30}$ of 760 m/s. For a discussion of this alternative one-step approach, the reader is directed to the report by Rodriguez-Marek, Ake, *et al.* (2021).

This article begins with an overview of the CY14 model, identifying the individual terms to be adjusted. Then the article describes two adjustments for the CY14 model that are not region-specific but rather are related to features of how this model was derived. The first adjustment corresponds to the long-period response spectral ordinates, recognizing the approach adopted by Chiou and Youngs (2014) regarding usable data at long periods was unique among the NGA-West2 models, all of which predict systematically larger accelerations at long (>5 s) periods. The second adjustment corresponds to the scaling for normal-faulting earthquakes, which is relevant to the INL study, because the site is located with the Basin and Range extensional province. The dataset used to derive the CY14 model contained very few recordings from normal events for which reason scaling for this type of rupture is uncertain due to the poor constraint.

The adjustments for source (stress parameter $\Delta\sigma$) and path (anelastic attenuation quality factor $Q$) parameters representative of the INL region are then presented, including the estimation of the target-region values and their associated uncertainty. For each adjustment, we discuss example weights of the logic-tree branches used to capture the epistemic uncertainty of the adjustments. The logic-tree branches and the weights for all the adjustments considered in this article are given in the final figure of the main body of this article.

This article concludes with a brief discussion of how the resulting range of epistemic uncertainty could be evaluated and the options for broadening the distribution, if required.

The intent of this article is to demonstrate the process of possible adjustments to a well-known backbone GMPM. The results are not intended for direct application, so tables of coefficients are not provided unless needed as part of the exposition.

## THE CY14 EQUATIONS AND TERMS TO BE ADJUSTED

For the purposes of this article, it is useful to break the CY14 function for the reference rock motion ($y_{\text{ref}}$) into parts that represent the different physical processes that contribute to the ground motion, as in the following equation:

$$\ln y_{\text{ref}} = F_C + F_{\text{SoF}} + F_S + F_{\text{GS}} + F_A + F_{\text{Ztor}} + F_{\text{Dip}} + F_{\text{DPP}} + F_{\text{HW}}, \quad (1)$$

in which the terms are functions for the effects of style-of-faulting ($F_{\text{SoF}}$), source ($F_S$), geometrical spreading ($F_{\text{GS}}$), path ($F_A$), depth to top of rupture ($F_{\text{Ztor}}$), fault dip ($F_{\text{Dip}}$), directivity ($F_{\text{DPP}}$), and hanging wall ($F_{\text{HW}}$); $F_C$ is a metadata-independent function. Equation (1) gives the motion for a reference rock condition ($V_{S30}$ = 1130 m/s in CY14). Because they use metadata that are the most used in applications, and for which it is possible to make adjustments from analysis of data in the INL region, we consider only the first five terms in this article. They are defined by the following equations:

$$F_C = c_1, \quad (1a)$$

$$F_{\text{SoF}} = \left\{c_{1a} + \frac{c_{1c}}{\cosh[2\max(\mathbf{M} - 4.5, 0)]}\right\} F_{\text{RV}} + \left\{c_{1b} + \frac{c_{1d}}{\cosh[2\max(\mathbf{M} - 4.5, 0)]}\right\} F_{\text{NM}}, \quad (1b)$$

$$F_S = c_2(\mathbf{M} - 6) + \frac{c_2 - c_3}{c_n}\ln[1 + e^{c_n(c_M - \mathbf{M})}], \quad (1c)$$

$$F_{\text{GS}} = c_4 \ln\{R_{\text{RUP}} + c_5 \cosh[c_6 \max(\mathbf{M} - c_{\text{HM}}, 0)]\} + (c_{4a} - c_4)\ln\left(\sqrt{R_{\text{RUP}}^2 + c_{\text{RB}}^2}\right), \quad (1d)$$

$$F_A = \gamma R_{\text{RUP}}, \quad (1e)$$

in which $\gamma$ is an anelastic attenuation parameter given by

$$\gamma = c_{\gamma 1} + \frac{c_{\gamma 2}}{\cosh[\max(\mathbf{M} - c_{\gamma 3}, 0)]}. \quad (1f)$$

In these equations, $\mathbf{M}$ is the moment magnitude; $R_{\text{RUP}}$ is the rupture distance; $F_{\text{RV}}$ and $F_{\text{NM}}$ are indicator variables for reverse and normal faulting, respectively; and all $c$ parameters

(with various subscripts) are model coefficients. The definitions of the other four terms ($F_{Ztor}$, $F_{Dip}$, $F_{DPP}$, and $F_{HW}$) can be inferred by comparing the definitions in equation (1) with equation (11) of CY14. The effects of site conditions are given in equation (12) of CY14, and CY14 should be consulted for the values of the coefficients appearing in equation (1). Period dependence is implicit in the functions. In addition, all but $F_C$ are dependent on metadata of some sort (style of faulting, depth to top of rupture, fault dip, magnitude, and distance measures).

The physical processes that are most likely to produce regional-dependent differences in the ground motion are: (1) the amplitude and frequency content radiated from the earthquake sources and (2) the effect of propagation from the source to the site. These contributors to the ground shaking are represented by $F_S$ for the source, and $F_{GS}$ and $F_A$ for the path. The path dependence is separated here into geometrical spreading and anelastic attenuation, respectively, for convenience in later discussions. For reasons discussed in the section on $F_A$, we only consider host-to-target path adjustments for $F_A$ and not $F_{GS}$.

All adjustments to a backbone GMPM can have epistemic uncertainties. One of the advantages of the CY14 GMPM is that these uncertainties can be taken into account by branches in a logic tree. We illustrate how this can be done for four functions in the CY14 GMPM for which we discuss adjustments: the metadata-independent function $F_C$, the style-of-faulting function $F_{SoF}$, the source function $F_S$, and the path function $F_A$.

## NONREGIONALLY DEPENDENT ADJUSTMENTS

### $F_C$ metadata-independent function

Chiou and Youngs (2008) found period-to-period discontinuities in the coefficient $c_1$ at longer periods that matched drops in the number of usable records due to filtering, from which they concluded that the long-period estimates of $c_1$ are biased to stronger motions; they removed this bias by imposing a smooth variation in the slope of $c_1$ with respect to period. This was a postregression adjustment. Consequently, CY14 tends to predict lower long-period ordinates relative to the other NGA-West2 models, as shown in Figure 1. To define the epistemic uncertainty, an adjustment to CY14 can be made for the long periods, and this adjustment can be given a weight in a branch of the logic tree. A method for defining the adjustment is as follows. Examples of the steps for **M** 6.5 are shown in Figure 2.

- Compute the 5%-damped pseudo-acceleration response spectra (PSA) from four NGA-West2 GMPMs for $R_{RUP}$ from 1 to 100 km, **M** from 5 to 8, and strike-slip (SS) earthquakes for a set of 22 oscillator periods with spacing from 0.008 to 10 s. The period spacing is approximately logarithmic.
- Calculate the geometric mean of the PSA, $PSA_{GMEAN}$, from Abrahamson *et al.* (2014; hereafter, ASK14); Boore *et al.* (2014; hereafter, BSSA14); and Campbell and Bozorgnia (2014; hereafter, CB14) for each set of **M**, $R_{RUP}$, and spectral period $T$.
- Calculate $\ln(PSA_{GMEAN}/PSA_{CY14})$, in which $PSA_{GMEAN}$ is computed in the previous step, and $PSA_{CY14}$ is the PSA for CY14 evaluated for the set of **M**, $R_{RUP}$, and $T$; the result is shown in Figure 2a.
- For each **M** and $R_{RUP}$, fit the period-dependent function $C + \Delta c_1$ to $\ln\frac{PSA_{GMEAN}}{PSA_{CY14}}$, in which $C$ is a period-independent constant, and $\Delta c_1$ is an adjustment term given by

$$\Delta c_1 = S \times \max\left\{\ln\left(\frac{T}{T_B}\right), 0\right\}^2, \tag{2}$$

in which $T_B$ is a magnitude-dependent threshold period given by $T_B = 2 - \max(0, \mathbf{M} - 7)$; $\Delta c_1 = 0$ for periods less than $T_B$. $\Delta c_1$ is plotted in Figure 2b for six distances and $\mathbf{M} = 6.5$.

The $S$ in equation (2) depends on distance and magnitude, as given in the following four equations:

$$S = S_1 + \frac{S_2}{\cosh(S_3 \times R_{RUP})}, \tag{3a}$$

$$S_1 = 0.2704 - 0.0694 \times \max(\mathbf{M} - 7, 0), \tag{3b}$$

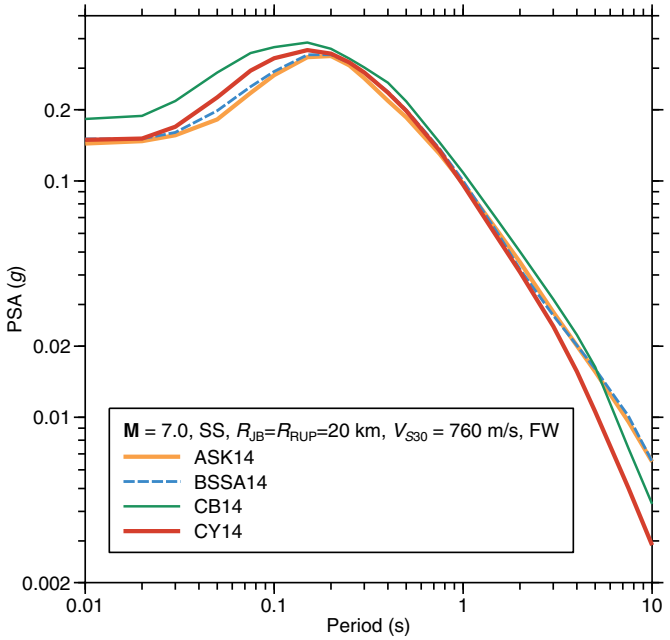


**Figure 1.** 5%-Damped pseudo-acceleration response spectra (PSA) as a function of period for four NGA-West2 project ground-motion prediction models (GMPMs) for the predictor variables shown in the legend (SS, strike slip; FW, footwall). ASK14, Abrahamson *et al.* (2014); BSSA14, Boore *et al.* (2014); CB14, Campbell and Bozorgnia (2014); CY14, Chiou and Youngs (2014). The color version of this figure is available only in the electronic edition.

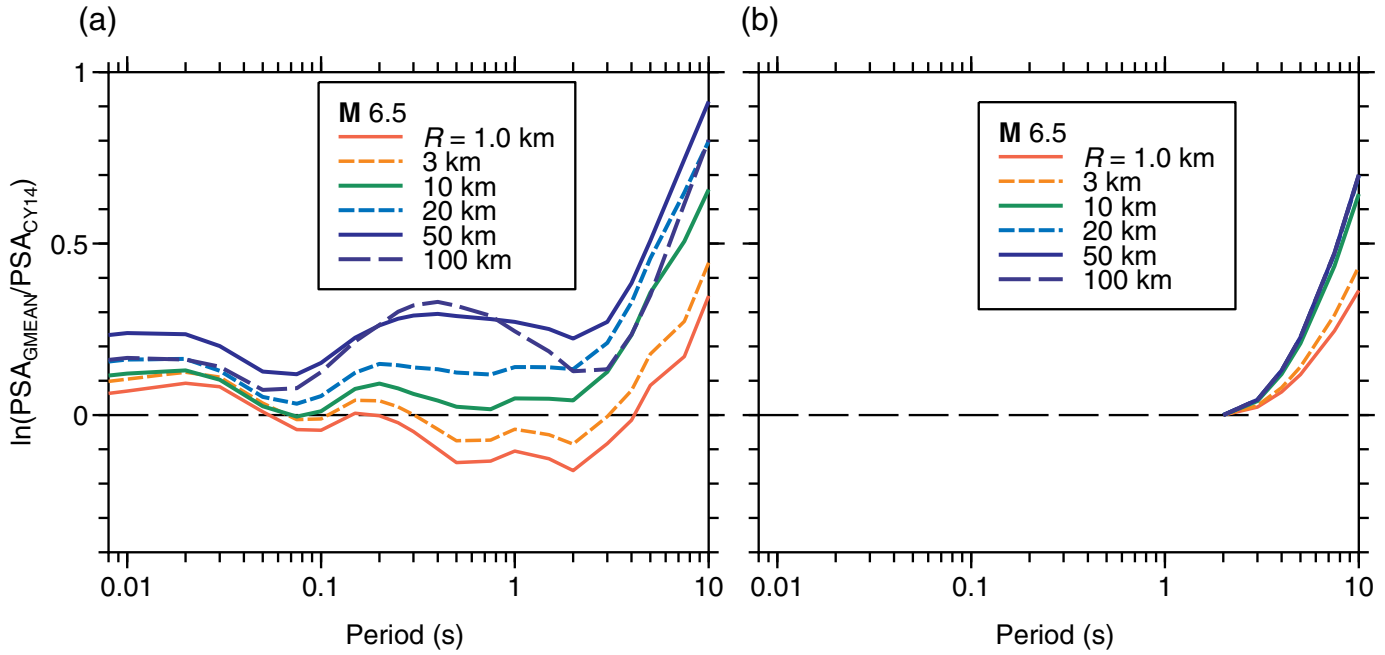


**Figure 2.** (a) Ratio of the geometric mean of PSA from ASK14, BSSA14, and CB14 to the PSA from CY14. (b) The $\Delta c_1$ adjustments to $F_C$. The color version of this figure is available only in the electronic edition.

$$S_2 = -0.1342 + 0.0716 \times \max(\mathbf{M} - 7, 0), \quad (3c)$$

$$S_3 = 0.2513 - 0.0419 \times \max(\mathbf{M} - 7, 0). \quad (3d)$$

The adjusted function for $F_C$ thus becomes

$$F_C = c_1 + \Delta c_1. \quad (4)$$

The logic tree for $F_C$ has two branches: one with $\Delta c_1 = 0$ and one with $\Delta c_1$ given by equation (2). It is reasonable to use weights of 0.5 for each branch as a default condition. On the other hand, it could be argued that there were good reasons for CY14 to expect a long-period bias and that the other three GMPMs (ASK14, BSSA14, and CB14) are not independent in that they used similar data and did not consider a post-regression adjustment for a bias in the long-period PSA. In this case, more weight could be given to the branch for which $\Delta c_1 = 0$.

## $F_{SoF}$ style-of-faulting function

Of the 300 earthquakes in the database used to derive CY14, only eight were normal-slip (NS) events. The constraint on the coefficients for scaling for NS earthquakes is therefore rather weak. One way to address this issue is to look at the relative scaling of spectral accelerations for NS to SS earthquakes in several current GMPMs, and use these to infer possible adjustment factors to be applied to the $F_{NM}$ term in equation (1b). Figure 3a shows the NS/SS ratio for several recent GMPMs, including four of the NGA-West2 GMPMs and two models (Akkar *et al.*, 2014a,b; hereafter, Aea14,a,b and Bindi *et al.*, 2014a,b, hereafter, Bea14a,b) based largely on Pan-European data, with relatively more NS events than used in the NGA-West2 GMPMs. Not shown in Figure 3a is the NS/SS ratio from a recent GMPM using data from Greece (Boore *et al.*, 2020); the ratio for this model is very similar to that shown in Figure 3a for BSSA14, particularly for periods less than about 2 s. More than 50 NS earthquakes provided data used in the Boore *et al.* (2020) GMPM. The BSSA14 values are also similar to NS/SS ratios of 0.8 for peak ground acceleration (PGA) and 0.85 for peak ground velocity (PGV) for Greece, from equations (3a) and (4a) in Skarlatoudis *et al.* (2003), assuming that PGA and PGV are similar to PSA at periods of 0.01 and 1.0 s, respectively. There is a considerable variation in the NS/SS ratio, as shown in Figure 3a, although three of the four NGA-West2 models are similar for periods less than about 1 s. A convenient way to capture some of the uncertainty shown in Figure 3a is to multiply $F_{NM}$ by a factor $\alpha_{NM}$, in which that factor is defined as follows:

- $\alpha_{NM} = 1$. No change to CY14 scaling; consistent with three NGA-West2 models (at short periods), although all are deficient in normal-faulting data.
- $\alpha_{NM} = 0$. Implies no difference between NS and SS motions; this is consistent with the Bea14a,b, Spudich *et al.* (1996) and Spudich *et al.* (1999, with an erratum given by Spudich and Boore, 2005) GMPMs for extensional regions.
- $\alpha_{NM} = \frac{1}{2}$. Model that lies between these two end members; consistent with ASK14 (at short periods) and Aea14a,b.

The adjusted NS/SS ratios for the CY14 GMPM using these factors are shown in Figure 3b for two magnitudes (the ratio is unity when $\alpha_{NM} = 0$ and therefore is independent of magnitude).

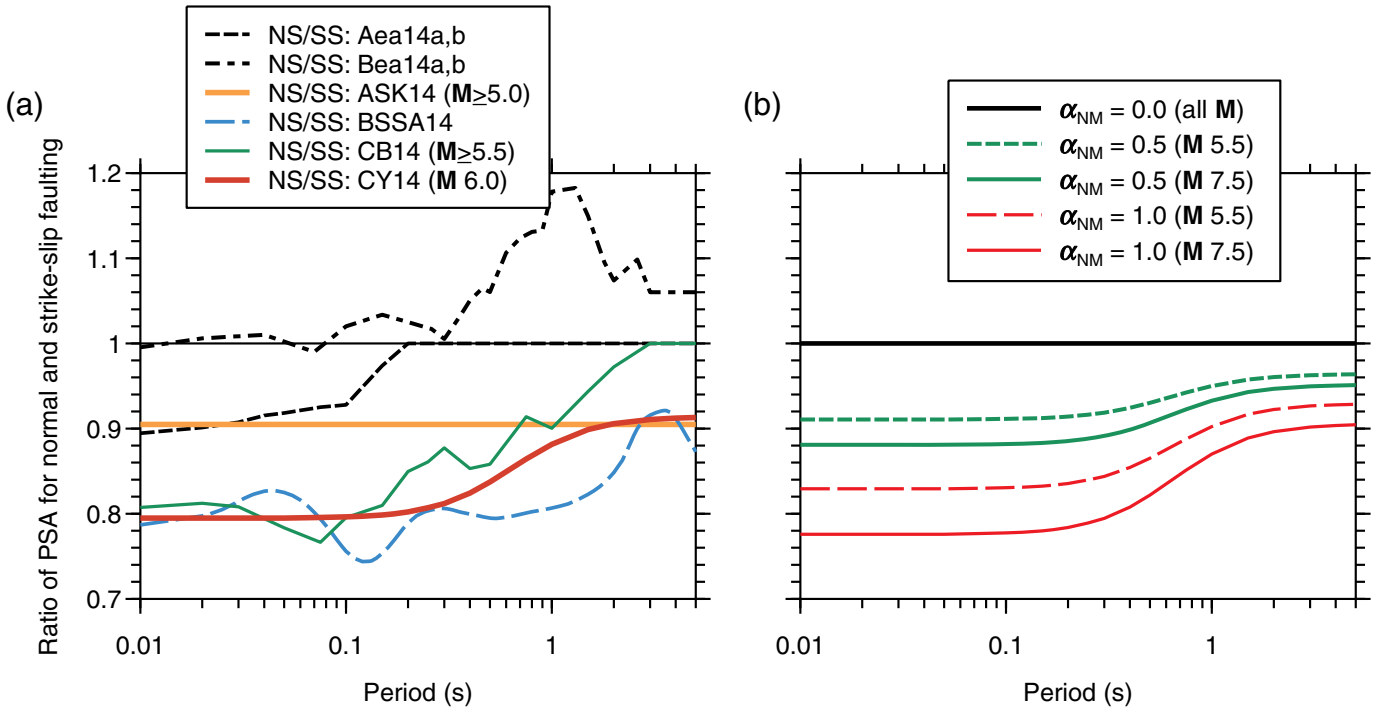


**Figure 3.** (a) Ratios of PSA for normal-slip and strike-slip earthquakes for a number of GMPMs. Aea14a,b, Akkar *et al.* (2014a,b) and Bea14a,b, Bindi *et al.* (2014a,b); the other acronyms are defined in the caption to Figure 1. (b) The CY14 style-of-faulting (SoF) adjustment as modified by the additional term given by $\alpha_{NM}$ for two magnitudes. The color version of this figure is available only in the electronic edition.

The adjusted function for $F_{SoF}$ is given by equation (5):

$$F_{SoF} = \left\{c_{1a} + \frac{c_{1c}}{\cosh[2\max(\mathbf{M} - 4.5, 0)]}\right\} F_{RV} + \left\{c_{1b} + \frac{c_{1d}}{\cosh[2\max(\mathbf{M} - 4.5, 0)]}\right\} \alpha_{NM} F_{NM}. \quad (5)$$

No adjustment is included for the $F_{RV}$ term, because there are no reverse-slip earthquakes for the target region used in this article.

With the formulation in this section, there are three logic-tree branches corresponding to $\alpha_{NM} = 0$, ½, and 1. As most of the GMPMs predict NS motions to be less than SS motions (Fig. 3a), it is reasonable to give less weight to the $\alpha_{NM} = 0$ branch than the other two branches. A possible set of weights is 0.2, 0.4, and 0.4 for the $\alpha_{NM} = 0$, ½, and 1 logic-tree branches, respectively.

## REGIONALLY DEPENDENT ADJUSTMENTS

Regionally dependent adjustments are made to the $F_S$ and $F_A$ functions. The adjustments use parameters obtained from inversions of ground-motion data recorded in the target-region. Before describing the adjustments, we first discuss briefly the target-region data and the inversion process.

### Data

The data used in the inversions are FAS computed from data recorded by a number of networks, including U.S. Geological Survey networks, INL Seismic Monitoring Program, Intermountain West Seismic Network, U.S. National Seismic Network, University of Utah Regional Seismic Network, and the USArray Transportable Array. The data included horizontal-component records from accelerometers and broadband instruments (as well as a few short-period instruments). The data were processed uniformly using the procedures developed for use in various Next Generation Attenuation (NGA) projects; the processing procedures are described in Ancheta *et al.* (2014). The logarithmically smoothed, vector-summed FAS from each recording used in the inversions have been adjusted for estimates of the smoothed site response, as described in the next paragraph. Details about the data selection, processing, and site amplifications are in Silva *et al.* (2021). The magnitude–distance distribution resulting from the selection process is shown in Figure 4. Data both inside (shown by squares in the figure) and outside the INL footprint were used. It is clear that the bulk of the data are for earthquakes less than magnitude 5, at distances beyond 100 km. On the other hand, except for long periods, most of the seismic hazard at INL comes from earthquakes greater than magnitude 5 and distances less than 100 km. Because the available data are not for the hazard-significant magnitudes and distances, there will be significant epistemic uncertainty in the adjustment factors.

Estimated site amplifications were removed from the FAS before they were used in the inversion process. The theoretical

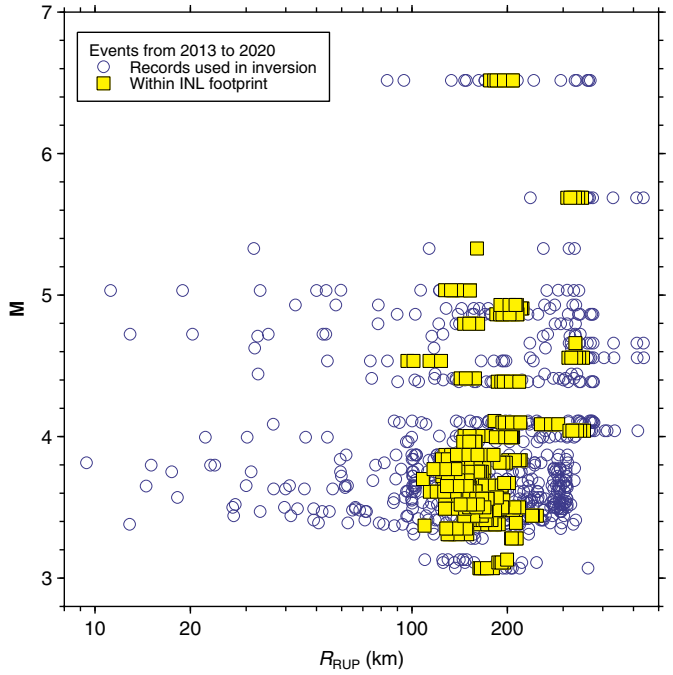


**Figure 4.** The magnitude–distance distribution of earthquakes in the target region around the Idaho National Laboratory (INL) used in the inversion to obtain parameters for the target region. The color version of this figure is available only in the electronic edition.

site amplifications for seven INL sites were computed using measured shear-wave velocity profiles at those sites after removal of any near-surface soil layers. The amplifications were smoothed over frequency before they were used to adjust the FAS. The amplifications for the sites without a velocity profile were based on the similarity of empirical site terms, determined from mixed effects regression analysis, with the empirical site terms at the seven INL stations. Cluster analysis was used to group sites with similar empirical site terms, and these groups were related to one of the seven INL sites on the basis of the closeness to one another on a Sammon's map (e.g., Scherbaum *et al.*, 2010; Goulet *et al.*, 2018). More details concerning the estimation of site amplifications are in Silva *et al.* (2021).

## Inversion process

The adjustments to the CY14 backbone GMPM are based on parameters that describe the FAS of the target-region data. The parameters were obtained using Markov chain Monte Carlo (MCMC) methods in a three-step process. The MCMC method is used because of its flexibility, while also including information through Bayesian inference and prior distributions. The starting model used the Stafford *et al.* (2022; hereafter, Sea22) optimal model parameters.

- Solve for the event-specific stress parameters ($\Delta\sigma$, the parameter controlling the amplitude of high-frequency radiation from the source; see Boore, 1983), the parameters describing the $Q$ model, and the site-specific kappa ($\kappa_0$) attenuation parameter (to a first approximation, $\kappa_0$ is presumed to be the value of the high-frequency spectral decay parameter $\kappa$ at zero distance, because the frequency-dependent attenuation of motion with distance has been accounted for by the $Q$ model).
- Using the site-specific $\kappa_0$ values from the previous step, fit the model again to obtain $\Delta\sigma$ and the $Q$ model.
- Using the site-specific $\kappa_0$ from step 1 and the $Q$ model from step 2, solve for the event-specific stress parameters $\Delta\sigma$.

A common challenge in the development of ground-motion models is the potential for parameters to trade-off with one another. This is especially the case when data are available in only a limited range of the domain (e.g., small range of distances). The procedure we used incrementally inverts for the parameters to isolate the influence of the specific parameter. The resulting stress parameters and $Q$ model are discussed in the following sections.

## $F_S$ source function

The Appendix shows that $F_S$ can be easily modified to account for differences in host- and target-region stress parameters $\Delta\sigma$. The modified equation for $F_S$ is given by equation (A4), repeated here:

$$F_S = c_2(\mathbf{M}-6) + \frac{c_2-c_3}{c_n}\ln[1+e^{c_n(c_M+\Delta c_M-\mathbf{M})}] - (c_2-c_3)\Delta c_M, \tag{6}$$

in which the difference in the coefficient $c_M$ for the two regions ($\Delta c_M$) is related to the ratio of the stress parameters for the regions, as given by equation (A19) in the Appendix, repeated here for convenience:

$$\Delta c_M = \chi_{\mathrm{FS2RS}}\frac{2}{3}\log\frac{\Delta\sigma_2}{\Delta\sigma_1}, \tag{7}$$

in which "1" and "2" refer to the host and target regions, respectively, and $\chi_{\mathrm{FS2RS}}$ is a period-dependent factor (given in the Appendix) that accounts for differences in the slopes of the magnitude scaling for Fourier spectra (FS) and response spectra (RS).

Stafford *et al.* (2022) inverted the CY14 GMPM to determine various parameters that can be used to predict the FAS in the host region. (The base-10 logarithm is used in equation (7), because it comes from a derivation that uses the standard relation between seismic moment and moment magnitude given in equation (A7), which is in terms of the base-10 logarithm; the rest of the logarithms in this article, denoted by the notation "ln", are base-$e$ logarithms.) The parameters determined by Sea22 include $\Delta\sigma_1$ and path parameters (used in the section discussing adjustments to $F_A$). Sea22 found that $\Delta\sigma_1$ increases with **M** up to **M** 5.0, after which it is constant. We assume that the

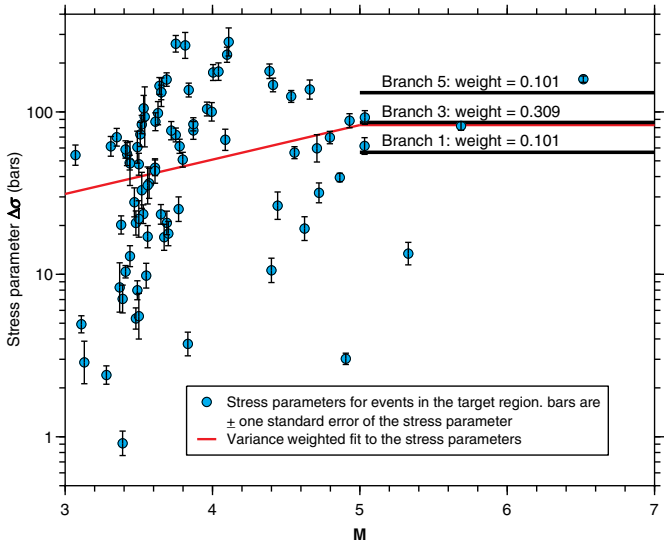


**Figure 5.** Stress parameters obtained by inverting the Fourier acceleration records from the target region. The lines are from a variance-weighted fit to the function in equation (8). The values of $\Delta\sigma_{\mathbf{M}5}$ for the lowest, middle, and the highest logic-tree branches are also shown for comparison. The color version of this figure is available only in the electronic edition.

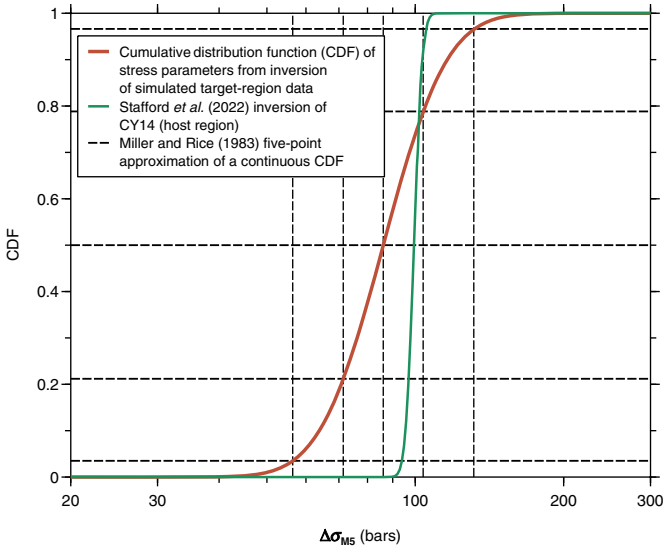


**Figure 6.** The cumulative distribution function (CDF) of $\Delta\sigma_{\mathbf{M}5} = \Delta\sigma(\mathbf{M} = 5)$ from the host region (CY14) and from inversions of the simulated target region stress-parameter data. The $\Delta\sigma_{\mathbf{M}5}$ for the Miller and Rice (1983) five-point approximation (vertical dashed lines) are shown for the target region only. The color version of this figure is available only in the electronic edition.

same dependence occurs in the target region. The finding that the stress parameter is constant for $\mathbf{M} \geq 5.0$ is convenient, because most PSHAs in tectonically active areas use the minimum magnitude of 5.0, and therefore complications due to magnitude-dependent $\Delta\sigma$ can be avoided.

To obtain $\Delta\sigma_2$, we inverted FAS from data recorded in the region surrounding the INL. The inverted stress parameters are plotted against magnitude in Figure 5. Also included in that figure is a bilinear fit to the data, assuming the same functional dependence between $\Delta\sigma$ and $\mathbf{M}$ used in Sea22 but ignoring the depth dependence in the Sea22 equation. The function used in this article is given by equation (8):

$$\ln \Delta\sigma = s_\alpha + s_\beta \min(\mathbf{M} - 5, 0), \tag{8}$$

in which $s_\alpha$ and $s_\beta$ are regression coefficients. We could use $\exp(s_\alpha)$ as $\Delta\sigma_2$ in equation (7), but there is so much scatter in the inverted stress parameters that a more sophisticated approach is needed. We used the following steps:

- Simulate many (4000 in this article, as the computations are very rapid) datasets of $\Delta\sigma$ values for the earthquakes used to obtain the stress parameters shown in Figure 5, where the stress parameter for each event is generated randomly from a log-normal distribution for each dataset using the mean and standard error of the stress parameters from the inversion of the actual data.
- For each simulated dataset:
  - Fit equation (8) to the simulated values of $\Delta\sigma$.
  - Let $\Delta\sigma_{\mathbf{M}5}$ denote the stress parameter for earthquakes with $\mathbf{M} \geq 5$. For a range of stress parameters $\Delta\sigma_{\mathbf{M}5}$ from 20 to 300 bars, compute the probability $p$ that each value of $\Delta\sigma_{\mathbf{M}5}$ would be less than or equal to the value expected from a normal distribution with a mean of $s_\alpha$ and a standard deviation given by the standard error of $s_\alpha$. This gives the cumulative distribution function (CDF) of $\Delta\sigma_{\mathbf{M}5}$ for each simulated dataset. As shown in Figure 6, this range was sufficient to define the CDF from 0 to 1.
- Compute the mean of $p$ over the 4000 datasets for each value of $\Delta\sigma_{\mathbf{M}5}$. This gives the average CDF for $\Delta\sigma_{\mathbf{M}5}$.
- Sample the CDF using the five-point Miller and Rice (1983) approximation to the CDF derived in the previous step.

Using the procedure given earlier, the CDFs of $\Delta\sigma_{\mathbf{M}5}$ for both the host region (computed from the Sea22 mean and standard error of $\Delta\sigma_{\mathbf{M}5}$) and the target region (from the procedure discussed in the bulleted list previously) are shown in Figure 6 as a function of $\Delta\sigma_{\mathbf{M}5}$. The horizontal dashed lines are the CDF values used in the five-point Miller and Rice (1983) approximation of the $\Delta\sigma_{\mathbf{M}5}$ CDF, and the vertical dashed lines are the corresponding $\Delta\sigma_{\mathbf{M}5}$ values for the target region (the vertical lines for the host region CDF are not shown to avoid clutter). The resulting discrete values of $\Delta\sigma_{\mathbf{M}5}$ from the host-region and the target-region inversions are used as $\Delta\sigma_1$ and $\Delta\sigma_2$, respectively, in computing $\Delta c_M$ using equation (6). The $\Delta c_M$ values are used with appropriate weights in the logic tree to capture the uncertainty in $F_S$. The results, including the

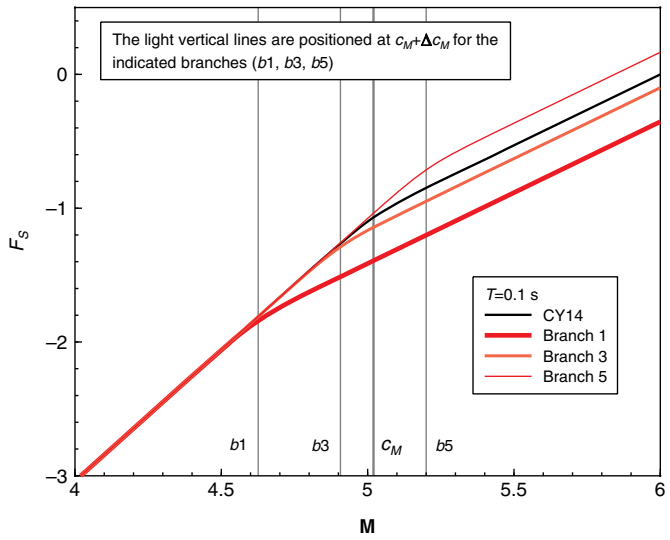


**Figure 7.** The target region source function $F_S$ for the lowest, middle, and the highest logic-tree branches. The adjusted hinge magnitude is shown for each branch, in which $\Delta c_M$ is calculated from the $\Delta\sigma_{\mathbf{M}5}$ for each branch. For comparison, also shown is $F_S$ for the host region (CY14). The color version of this figure is available only in the electronic edition.

TABLE 1
**Information Related to the Logic-Tree Branches for the $F_S$ Host-to-Target Adjustment to the CY14 GMPM for an Oscillator Period of 0.1 s**

| $T$(s) | Branch | CDF | $\Delta\sigma_{\text{Host}}$ | $\Delta\sigma_{\text{Target}}$ | $\Delta c_M$ | Weight |
|---|---|---|---|---|---|---|
| 0.1 | 5 | 0.96511 | 105.1 | 131.4 | 0.183 | 0.101 |
| 0.1 | 4 | 0.78830 | 101.9 | 103.8 | 0.015 | 0.244 |
| 0.1 | 3 | 0.50000 | 99.4 | 86.1 | −0.110 | 0.309 |
| 0.1 | 2 | 0.21170 | 96.9 | 71.4 | −0.234 | 0.244 |
| 0.1 | 1 | 0.03489 | 94.0 | 56.4 | −0.391 | 0.101 |

The units of $\Delta\sigma$ are bars. The branches are numbered from the smallest to the largest values of the $\Delta c_M$ adjustment. CDF, cumulative distribution function; CY14, Chiou and Youngs (2014); and GMPM, ground-motion prediction model.

logic-tree weights for the five branches, are given in Table 1 for an oscillator period of 0.1 s. To give an idea of the relation of the epistemic uncertainty in $\Delta\sigma_{\mathbf{M}5}$ to the scatter in the inverted stress parameters, $\Delta\sigma_{\mathbf{M}5}$ for the lowest, middle, and the highest logic-tree branches have been added to the plot of the $\Delta\sigma$ in Figure 5. The weights of the logic-tree branches are such that they and the associated values of $\Delta\sigma_{\mathbf{M}5}$ are a discrete representation of the continuous CDF for the host region and the target region; those values of $\Delta\sigma_{\mathbf{M}5}$ are used to compute the $\Delta c_M$ values, and therefore the logic-tree branches for $\Delta c_M$ have the same weights as the discrete $\Delta\sigma_{\mathbf{M}5}$ values.

The $F_S$ source function for the host and target region are plotted against **M** in Figure 7 for a period of 0.1 s. It is clear that the epistemic uncertainty in $\Delta\sigma_{\mathbf{M}5}$ leads to a large range in PSA values (but branches 1 and 5 have lower weights than branch 3, as shown in Fig. 5 and in Table 1).

## $F_A$ path function

We only consider host-to-target path adjustments for $F_A$ and not $F_{\text{GS}}$. We do this because $F_A$ and $F_{\text{GS}}$ are correlated such that various combinations can result in similar motions at distances that matter in engineering applications. With the available ground-motion datasets, it is difficult to isolate the two components independently. On the other hand, $F_A$ has little effect on ground motions at short-to-intermediate distances, so the usual approach in building GMPMs is to use data at those distances to determine $F_{\text{GS}}$ and then use that function at all distances, with $F_A$ being determined by more distant data. Recent GMPMs that allow for regional differences in the path effect on ground motions (e.g., ASK14, BSSA14, CB14, and CY14) assume that $F_{\text{GS}}$ is region independent, with regional differences in the path function being accounted for only in $F_A$.

The adjustments to $F_A$ (equation 1e) were derived by comparing simulated RS for models of the target-region and the host-region FAS, focusing on the parameters that control the attenuation with distance. The host-region FAS model comes from Sea22, whereas the target-region FAS uses the Sea22 geometrical spreading, with a target-region anelastic attenuation model $Y$ as parameterized by the function in equation (9):

$$Y = \exp[-(\pi f R_{\text{RUP}})/(Q c_Q)], \tag{9}$$

in which $f$ is frequency, and $c_Q$ is a shear-wave velocity, taken as 3.5 km/s both in Sea22 and in this article. $Q$ is the attenuation quality factor, given by

$$Q = Q_0 f^{\eta(\mathbf{M})}, \tag{10}$$

in which $Q_0$ is a regression parameter, and the magnitude-dependent exponent $\eta(\mathbf{M})$ is given by

$$\eta(\mathbf{M}) = \eta_\alpha + \eta_\beta \tanh(\mathbf{M} - \eta_\gamma). \tag{11}$$

In this equation, $\eta_\alpha$, $\eta_\beta$, and $\eta_\gamma$ are regression parameters.

The parameters $Q_0$, $\eta_\alpha$, and $\eta_\beta$ for the target region were determined from inversions of the target-region data; we judged that the available data were not adequate to determine $\eta_\gamma$, and therefore that parameter was taken as the Sea22 value (5.1278). A comparison of $Q$ is shown in Figure 8 for both the host region (from Sea22) and the target region (as determined from the inversions). Because $Q$ is magnitude dependent, values are shown for two magnitudes: 4.5 and 7.5. Figure 8 shows that the magnitude dependence of $Q$ is smaller for the target-region than it is for the host region ($\frac{\partial\eta}{\partial \tanh M} = 0.04$ and 0.14 for the target and host regions, respectively). There are enough small-magnitude data in the target-region dataset that we think the relatively small host- and target-region differences in $Q$ for small earthquakes are real region-specific differences and not

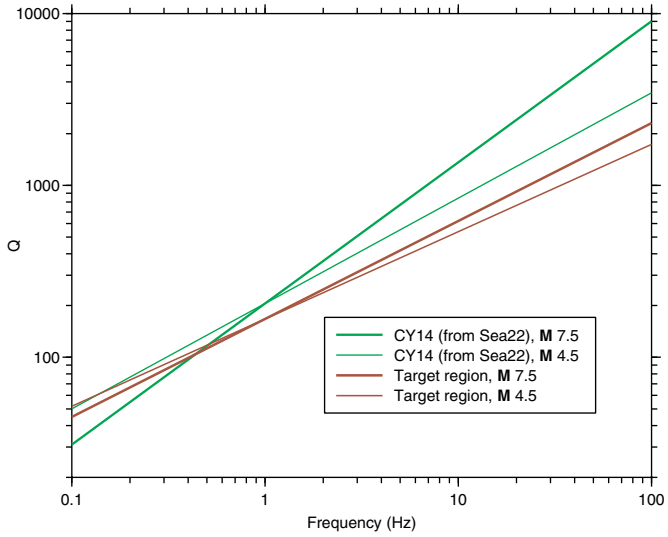


**Figure 8.** The $Q$ attenuation parameter using the mean $Q_0$, $\eta_\alpha$, $\eta_\beta$, and $\eta_\gamma$ from the Sea22 inversion of CY14 and from the regression analysis of the target-region data. The color version of this figure is available only in the electronic edition.

an artifact of limited data. The same cannot be said for the differences in $Q$ for larger earthquakes, however, as data for such events are lacking in the target region. We note that the determination of the anelastic attenuation parameter adjustment $\Delta\gamma$ uses the uncertainties in the $Q$ model parameters determined in the inversions.

The adjustments to $F_A$ and development of the logic-tree branches were determined using the following steps for each period of interest:

- Generate nsim random samples of $Q_0$, $\eta_\alpha$, $\eta_\beta$, and $\eta_\gamma$, using the mean values, standard errors, and correlation coefficients of the four parameters for both the Sea22 and INL-region inversions (nsim = 1000 in this example). The random samples were obtained using the R function mvrnorm (Venables and Ripley, 2002), which accounts for the correlation between the parameters.
- For each random sample of the $Q$ parameters:
  - Simulate PSA for the host and target regions. These simulations were performed for **M** 4.4–8.0, with a spacing of 0.1 units, and 21 values of $R_{JB}$ (Joyner–Boore distance), logarithmically spaced from 10 to 120 km. For the sake of illustration in this article, only a period of 0.1 s was considered, although the procedure applies to all periods. (An exception is for the branch corresponding to the mean value of the $\Delta\gamma$ adjustment, which can be made by using the mean values of the $Q$ parameters, without needing simulations for the large numbers of random samples of the $Q$ parameters.) The simulations were computed using the point-source stochastic model (Boore, 2005) with parameters from the Sea22 inversion of CY14. The $R_{JB}$ distance was converted to $R_{RUP}$ using the equation $R_{RUP} = \sqrt{R_{JB}^2 + Z_{TOR}^2}$, in which $Z_{TOR}$ (depth to top of rupture), a function of **M**, came from the CY14 model for SS and NS faulting (their equation 5). The simulated ground motions for the host region and target region are $PSA_{HOST}$ and $PSA_{TARGET}$, respectively. The parameter files used in the simulations are available in the supplemental material available to this article.
  - Compute the simulated adjustments $\Delta\gamma_{SIM}$ to the anelastic attenuation using equation (12):

$$\Delta\gamma_{SIM} = \ln\left(\frac{PSA_{TARGET}}{PSA_{HOST}}\right)/R_{RUP}. \qquad (12)$$

  - The result for simulations using the mean values of the $Q$ parameters is plotted in Figure 9a for a period of 0.1 s and magnitudes 4.5 and 7.5. There is some dependence of

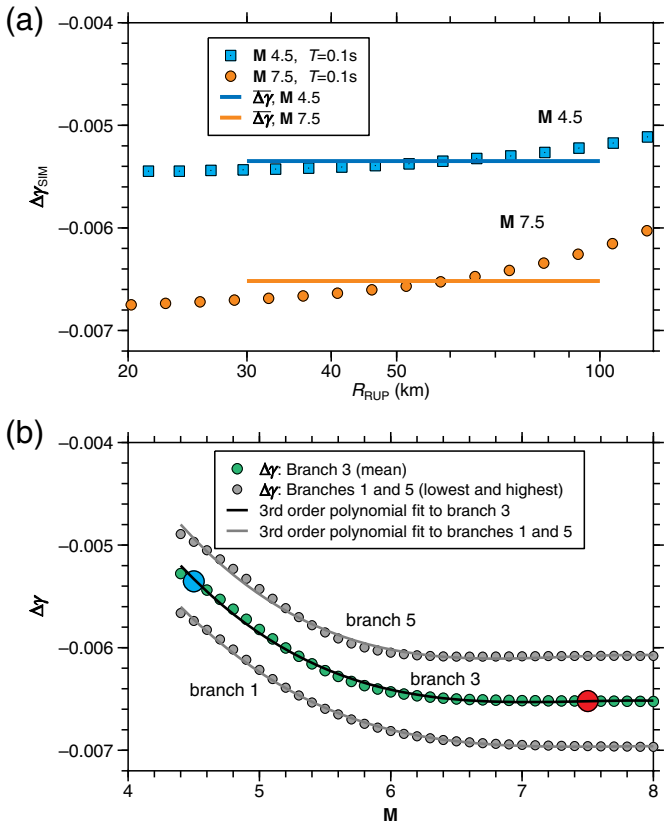


**Figure 9.** (a) The anelastic attenuation parameter $\Delta\gamma_{SIM}$ computed from the logarithm of the ratio of simulated PSA using mean parameters for the target region and for the CY14 GMPM for one period (0.1 s) and two magnitudes (4.5 and 7.5). The horizontal lines are averages of $\Delta\gamma$ from 30 to 100 km ($\overline{\Delta\gamma}$). (b) $\overline{\Delta\gamma}$ versus **M** for $T$ = 0.1 s for the lowest, middle, and the highest logic-tree branches (see Table 2). The two values for **M** 4.5 and 7.5 plotted using larger symbols correspond to the short horizontal lines in graph (a). The color version of this figure is available only in the electronic edition.

$\Delta\gamma_{SIM}$ on $R_{RUP}$, particularly, at greater distances. Because distances beyond 100 km are not important to the hazard at INL from crustal earthquakes, we ignore that dependence, focusing attention on the magnitude dependence. In other applications, however, it might be necessary to include a distance dependence in $\Delta\gamma$.

- For each magnitude, compute $\overline{\Delta\gamma}$—the average of $\Delta\gamma_{SIM}$ from 30 to 100 km. There will be nsim values of $\overline{\Delta\gamma}$ for each magnitude. The values for **M** 4.5 and 7.5 are shown as the horizontal lines in Figure 9a.

- For each value of **M**:
  - Find the mean and standard deviation of $\overline{\Delta\gamma}$ over all the simulations.
  - Use the five-point Miller and Rice (1983) procedure to sample the CDF corresponding to a normal distribution defined by the mean and standard deviation in the previous step. These values can be used as the $\Delta\gamma$ adjustments to the CY14 GMPM for the five branches of the logic tree. The values for all magnitudes are plotted in Figure 9b for the samples corresponding to the lowest, middle, and the highest values of the CDF samples.
  - Because of the magnitude dependence of $\Delta\gamma$ shown in Figure 9b, it is convenient for use in applications to fit a polynomial to $\Delta\gamma$ as a function of **M**. For the example given in this article, we found that the following equation was a reasonable fit to $\Delta\gamma$ as a function of **M**:

$$\Delta\gamma = c_0 + c_1(\mathbf{M} - 6) + c_2(\mathbf{M} - 6)^2 + c_3(\mathbf{M} - 6)^3. \quad (13)$$

This equation gives the adjustment $\Delta\gamma$ to the $F_A$ function given by equation (1e). The coefficients of the polynomial, $c_0$–$c_3$, are provided in Table 2 for the five branches of the logic tree, and the fits to **M** are shown in Figure 9b for three branches.

The revised function $F_A$ is now given by adding $\Delta\gamma$ from equation (13) to $\gamma$ in equation (1e):

$$F_A = (\gamma + \Delta\gamma)R_{RUP}. \quad (14)$$

A comparison of the host region $\gamma$ and the adjustment $\Delta\gamma$ is given in Figure 10 as a function of period for four magnitudes for the middle branch of the logic tree (the range for all branches for $T = 0.1$ s is shown by the bars on the value of $\Delta\gamma$ corresponding to that period). There is less magnitude dependence in $\Delta\gamma$ than in $\gamma$. In addition, $\Delta\gamma$ is negative for almost all periods and magnitudes, which means that the ground-motion intensity measures (GMIMs) decay more rapidly with distance in the target region than the host region, particularly, for short periods.

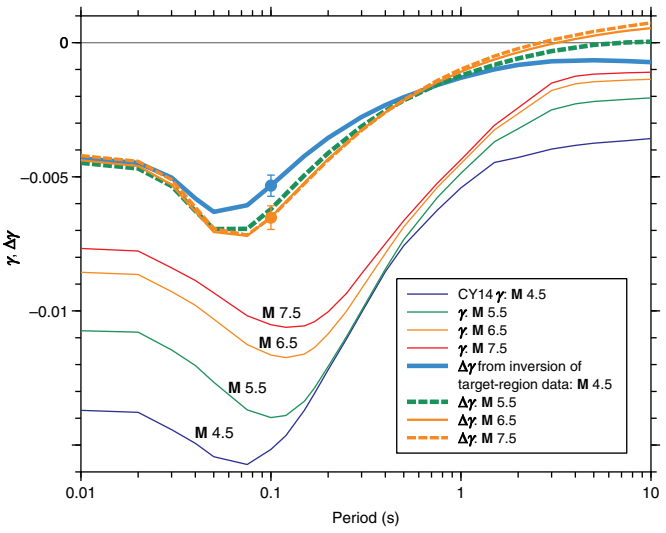


**Figure 10.** The anelastic attenuation ($F_A$) parameter $\gamma$ from CY14 and the adjustment $\Delta\gamma$ developed in this article for the middle logic-tree branch (the mean value of $\Delta\gamma$, which was developed using the mean values of the $Q$ parameters, without the need for multiple simulations). The results of using the 1000 simulations are shown by the symbols for $\Delta\gamma$ at $T = 0.1$ s, with the bars for $\Delta\gamma$ at $T = 0.1$ s corresponding to the lowest and the highest logic-tree branches. The target-region attenuation parameter is given by $\gamma + \Delta\gamma$. The color version of this figure is available only in the electronic edition.

As mentioned earlier, the simulations used all of the Sea22 optimal model parameters except for the $Q$ function. One of the parameters needed in the conversion from FAS to PSA is the distance dependence of the duration due to the propagation of waves from the source to the site. Sea22 used the Boore and Thompson (2014) model for the path component of the durations (the other component being the source duration). It is possible to validate this duration model using the INL-region data; but this was not done in this study.

TABLE 2
**Logic-Tree Branches for $F_A$**

| $T$ (s) | Branch | CDF | Weight | $c_0$ | $c_1$ | $c_2$ | $c_3$ |
|---|---|---|---|---|---|---|---|
| 0.1 | 5 | 0.96511 | 0.101 | $-6.018 \times 10^{-03}$ | $-2.559 \times 10^{-04}$ | $2.264 \times 10^{-04}$ | $-5.598 \times 10^{-05}$ |
| 0.1 | 4 | 0.78830 | 0.244 | $-6.236 \times 10^{-03}$ | $-2.735 \times 10^{-04}$ | $2.197 \times 10^{-04}$ | $-5.195 \times 10^{-05}$ |
| 0.1 | 3 | 0.50000 | 0.309 | $-6.409 \times 10^{-03}$ | $-2.874 \times 10^{-04}$ | $2.144 \times 10^{-04}$ | $-4.877 \times 10^{-05}$ |
| 0.1 | 2 | 0.21170 | 0.244 | $-6.582 \times 10^{-03}$ | $-3.013 \times 10^{-04}$ | $2.091 \times 10^{-04}$ | $-4.558 \times 10^{-05}$ |
| 0.1 | 1 | 0.03489 | 0.101 | $-6.800 \times 10^{-03}$ | $-3.189 \times 10^{-04}$ | $2.024 \times 10^{-04}$ | $-4.155 \times 10^{-05}$ |

The last four columns are coefficients of equation (13) giving $\Delta\gamma$ as a function of **M** for the various branches. The branches are numbered from the smallest to the largest values of the $\Delta\gamma$ adjustment. Although the results are for a single period (0.1 s), the procedure can be used without alteration to obtain the values in the table for any period.

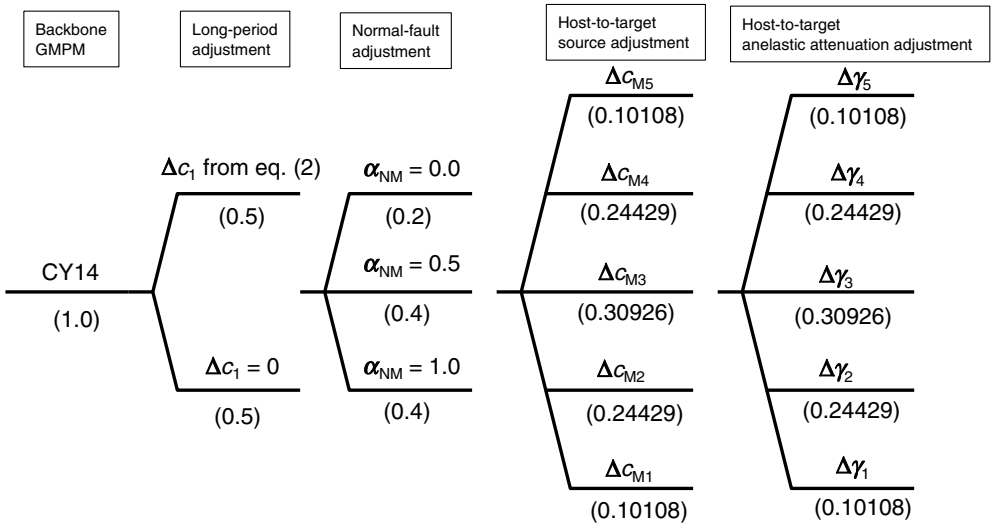


**Figure 11.** The complete logic tree for the four adjustments discussed in this article. The numbered subscripts for the source and anelastic attenuation branches correspond to the logic-tree branch numbers with parameter values given in Tables 1 and 2. The weights are given in parentheses below each branch.

## EPISTEMIC UNCERTAINTY IN THE RESULTING LOGIC TREE

The application of the adjustments for inherent features of the CY14 model that can be viewed as epistemic uncertainties (long-period spectral amplitudes and scaling for normal-faulting earthquakes) and for the two fundamental host-to-target source and site differences (median stress parameter and anelastic attenuation) lead to a logic tree with four nodes and a large number of branch combinations. The logic tree for the nodes and branches discussed in this article is shown in Figure 11. The branches are for $\ln y_{\text{ref}}$ (equation 1). The numbers in the subscripts for the two region-specific adjustments are the branch numbers from the bottom up, and correspond to the weights in Tables 1 and 2.

Recalling the objective of capturing the CBR of TDI, the final stage of completing the GMC logic tree is to assess whether the branches collectively capture a sufficiently broad range of epistemic uncertainty and, if not, to add nodes and/or branches to broaden the distribution of predicted ground-motion amplitudes. There is no direct way, by definition, to quantify the correct range of epistemic uncertainty, but comparisons can be made to guide and inform the expert judgement. For example, plots can be generated for appropriate ranges of magnitude and distance of the model-to-model variability of the median prediction from the GMC logic tree, and these can then be compared to similar plots for other suites of GMPMs that might be considered as a lower bound for the range of epistemic uncertainty. An obvious candidate for such a comparative baseline could be the model-to-model variability of the NGA-West2 GMPMs, which might be considered as a lower bound against which the target-region epistemic uncertainty could be compared. However, this may not be as straightforward as it sounds, for a number of reasons. First, the model-to-model variability of the NGA-West2 equations is found to diminish with increasing magnitudes, which is counterintuitive since the uncertainty would be expected to increase in the magnitude range where data are sparser. Second, the comparison of the GMC logic tree for the INL-region site with the NGA-West2 models warrants careful consideration, because the latter applies to a much larger region (and indeed combines data from several regions), and the site characterization data available for the NGA-West2 database are generally inferior to the detailed site information gathered for the target locations at INL. Nonetheless, taken at face value, the comparisons suggested that, overall, the level of uncertainty in the INL-region model is equal to or greater than that represented by the NGA-West2 models. However, the true range of epistemic uncertainty in the NGA-West2 models should include the additional intra-model uncertainty proposed by Al Atik and Youngs (2014; hereafter, AAY14) in the predictions of the median GMIMs, based on the density of the database in different magnitude–distance bins. The AAY14 model for additional epistemic uncertainty could therefore be added as a fifth node to the INL-region logic tree; this would be similar to the epistemic uncertainty branches shown in figure 10 of AAY14. The AAY14 model includes epistemic uncertainty for SS and reverse ruptures (taken together), as well as for normal-faulting earthquakes. Although the latter model leads to greater increases of epistemic uncertainty, to reflect the relative paucity of recordings from normal-faulting earthquakes in the NGA-West2 database, we suggest using the uncertainties for only the SS and reverse faulting cases, as the deficiency due to the lack of normal-faulting data has already been addressed in the INL-region logic tree through the node for normal-faulting factors.

In assessing the epistemic uncertainty captured by the GMC logic tree for the INL target region, it is important to bear in mind that it only captures the epistemic uncertainty in the reference rock motions. The reference rock hazard could be convolved with site adjustment factors that are developed to capture the full range of epistemic uncertainty in the site response characteristics (Rodriguez-Marek, Bommer, *et al.*,

2021), in which case the total epistemic uncertainty in the surface hazard at the target horizons would be represented by the combination of the uncertainty in the rock motions and the uncertainty in the site adjustment factors.

## DISCUSSION AND CONCLUSIONS

For site-specific PSHA studies, we believe that it would now be difficult to justify the continued approach of building the ground-motion logic tree by populating the branches with published GMPMs selected and weighted on the basis of their potential applicability to the target region. A superior approach is to select a backbone GMPM chosen for being amenable to host-to-target-region adjustments rather than any inherent applicability to the target region and to then construct the logic tree as a series of nodes for the individual adjustments for host-to-target-region differences in source and path parameters. We recognize that the method described in this article would be a challenge to apply either for hazard analyses over broad regions or for sites with very limited data on which to base host-to-target adjustments.

This article has been built on the work of Bommer and Stafford (2020), in which CY14 was identified as the most suitable of all current GMPMs for shallow crustal earthquakes in terms of its adaptability through individual adjustments for host-to-target-region differences in source (stress parameter $\Delta\sigma$) and path (anelastic attenuation quality factor $Q$) characteristics. Subsequent work by Al Atik and Abrahamson (2021) provided a $V_S$ profile and $\kappa_0$ consistent with rock ($V_{S30} = 760$ m/s) predictions from CY14, which Stafford *et al.* (2022) used to invert the CY14 for model-consistent estimates of the stress parameter $\Delta\sigma$ and the attenuation quality factor $Q$. In this study, these host-region characteristics have been used as the starting point for the construction of a logic tree for ground-motion predictions in reference rock for the INL using target-region estimates of $\Delta\sigma$ and $Q$ obtained from analysis of local and regional ground-motion recordings. The logic tree also includes nodes for adjustments that address the lack of constraint for normal-faulting earthquakes in the CY14 database and the unique treatment of long-period spectral ordinates in the derivation of that model. In addition, for the INL study it was decided to include an additional node to impose the additional epistemic uncertainty proposed by Al Atik and Youngs (2014) for the NGA-West2 models, given that this should be applied in the host region and therefore cannot be omitted from the target region.

In the future, we expect new GMPMs to be published that are as suitable for host-to-target adjustments as the CY14 model and possibly superior in other regards such as including better constraints on normal-faulting earthquake ground motions. Until such time, however, the procedure illustrated herein could be applied to any site-specific PSHA in regions of shallow crustal seismicity, which could significantly simplify the construction of the ground-motion logic tree for reference rock motions. Adopting this framework, with CY14 as the backbone GMPM, the host-region characteristics are now readily available, and the methodology for making host-to-target-region adjustments have been explained. The ground-motion model-building component of any site-specific PSHA project can therefore focus almost exclusively on the estimation of target-region source and path parameters, and then on the adjustment from reference rock profile of CY14 to the target site profile.

## DATA AND RESOURCES

The site-amplification-adjusted, logarithmically smoothed, vector-summed Fourier amplitude spectra (FAS) used in the inversions are included in the supplemental material. The figures were prepared using CoPlot (www.cohortsoftware.com). The simulations needed for the $F_S$ and $F_A$ adjustments were computed using *tmrsk_loop_rv_drvr* and *tmrsk_loop_rv_drvr_for_random_samples_of_Sea22_Q_params* programs included in the SMSIM suite of programs (Boore, 2005) available from the online software link on http://www.daveboore.com. Most of the analysis used scripts written in the statistical language and environment R (R Core Team, 2022; https://www.R-project.org/). All websites were last accessed in July 2022. Inversions were performed using pymc3 (Salvatier *et al.*, 2016). The supplemental material for this article includes the site-amplification-adjusted FAS used in this study for the INL region, and the parameter and control files used in the simulations.

## DECLARATION OF COMPETING INTERESTS

The authors acknowledge that there are no conflicts of interest recorded.

## ACKNOWLEDGMENTS

The authors thank Carola Di Alessandro, John Douglas, and an anonymous reviewer for useful reviews.

## REFERENCES

Abrahamson, N. A., W. J. Silva, and R. Kamai (2014). Summary of the ASK14 ground motion relation for active crustal regions, *Earthq. Spectra* **30,** 1025–1055.

Ake, J., C. Munson, J. Stamatakos, M. Juckett, K. Coppersmith, and J. Bommer (2018). Updated implementation guidelines for SSHAC hazard studies, *U.S. Nuclear Regulatory Commission, NUREG-2213*, 145 pp.

Akkar, S., M. A. Sandıkkaya, and J. J. Bommer (2014a). Empirical ground-motion models for point- and extended-source crustal earthquake scenarios in Europe and the Middle East, *Bull. Earthq. Eng.* **12,** 359–387.

Akkar, S., M. A. Sandıkkaya, and J. J. Bommer (2014b). Erratum to: Empirical ground-motion models for point- and extended-source crustal earthquake scenarios in Europe and the Middle East, *Bull. Earthq. Eng.* **12,** 389–390.

Al Atik, L., and N. Abrahamson (2021). A methodology for the development of 1D reference $V_S$ profiles compatible with ground-motion prediction equations: Application to NGA-West2 GMPEs, *Bull. Seismol. Soc. Am.* **111,** 1765–1783.

Al Atik, L., and R. R. Youngs (2014). Epistemic uncertainty for NGA-West2 models, *Earthq. Spectra* **30,** 1301–1318.

Ancheta, T. D., R. B. Darragh, J. P. Stewart, E. Seyhan, W. J. Silva, B. S. J. Chiou, K. E. Wooddell, R. W. Graves, A. R. Kottke, D. M. Boore, *et al.* (2014). NGA-West2 database, *Earthq. Spectra* **30,** 989–1005.

Atkinson, G. M., J. J. Bommer, and N. A. Abrahamson (2014). Alternative approaches to modeling epistemic uncertainty in ground motions in probabilistic seismic-hazard analysis, *Seismol. Res. Lett.* **85,** 1141–1144.

Bazzurro, P., and C. A. Cornell (2004). Nonlinear soil-site effects in probabilistic seismic-hazard analysis, *Bull. Seismol. Soc. Am.* **94**, 2110–2123.

Bindi, D., M. Massa, L. Luzi, G. Ameri, F. Pacor, R. Puglia, and P. Augliera (2014a). Pan-European ground-motion prediction equations for the average horizontal component of PGA, PGV, and 5%-damped PSA at spectral periods up to 3.0 s using the RESORCE dataset, *Bull. Earthq. Eng.* **12,** 391–430.

Bindi, D., M. Massa, L. Luzi, G. Ameri, F. Pacor, R. Puglia, and P. Augliera (2014b). Erratum to: Pan-European ground-motion prediction equations for the average horizontal component of PGA, PGV, and 5%-damped PSA at spectral periods up to 3.0 s using the RESORCE dataset, *Bull. Earthq. Eng.* **12,** 431–448.

Bommer, J. J. (2012). Challenges of building logic trees for probabilistic seismic hazard analysis, *Earthq. Spectra* **28,** 1723–1735.

Bommer, J. J., and F. Scherbaum (2008). The use and misuse of logic trees in probabilistic seismic hazard analysis, *Earthq. Spectra* **24,** 997–1009.

Bommer, J. J., and P. J. Stafford (2020). Selecting ground-motion models for site-specific PSHA: Adaptability versus applicability, *Bull. Seismol. Soc. Am.* **110,** 2801–2815, doi: 10.1785/0120200171.

Boore, D. M. (1983). Stochastic simulation of high-frequency ground motions based on seismological models of the radiated spectra, *Bull. Seismol. Soc. Am.* **73,** 1865–1894.

Boore, D. M. (2003). Simulation of ground motion using the stochastic method, *Pure Appl. Geophys.* **160,** 635–676.

Boore, D. M. (2005). SMSIM—Fortran programs for simulating ground motions from earthquakes: Version 2.3—A revision of OFR 96-80-A, *U.S. Geol. Surv. Open-File Rept. 00-509*, Revised 15 August 2005, 55 pp.

Boore, D. M., and E. M. Thompson (2014). Path durations for use in the stochastic-method simulation of ground motions, *Bull. Seismol. Soc. Am.* **104,** 2541–2552, doi: 10.1785/0120140058.

Boore, D. M., J. P. Stewart, E. Seyhan, and G. M. Atkinson (2014). NGA-West 2 equations for predicting PGA, PGV, and 5%-Damped PSA for shallow crustal earthquakes, *Earthq. Spectra* **30,** 1057–1085.

Boore, D. M., J. P. Stewart, A. Skarlatoudis, E. Seyhan, B. Margaris, N. Theodoulidis, E. Scordilis, I. Kalogeras, N. Klimis, and N. S. Melis (2020). A ground-motion prediction model for shallow crustal earthquakes in Greece, *Bull. Seismol. Soc. Am.* **111,** 857–874.

Campbell, K. W. (2003). Prediction of strong ground motion using the hybrid empirical method and its use in the development of ground-motion (attenuation) relations in eastern North America, *Bull. Seismol. Soc. Am.* **93,** 1012–1033.

Campbell, K. W., and Y. Bozorgnia (2014). NGA-West2 ground motion model for the average horizontal components of PGA, PGV, and 5% damped linear acceleration response spectra, *Earthq. Spectra* **30,** 1087–1115.

Chiou, B. S. J., and R. R. Youngs (2008). NGA model for average horizontal component of peak ground motion and response spectra, *PEER Rept. 2008/09*, Pacific Earthquake Engineering Research Center, University of California, Berkeley, California, 293 pp.

Chiou, B. S. J., and R. R. Youngs (2014). Update of the Chiou and Youngs NGA Model for the average horizontal component of peak ground motion and response spectra, *Earthq. Spectra* **30,** 1117–1153.

Goulet, C., Y. Bozorgnia, N. Abrahamson, N. Kuehn, L. Al Atik, R. Youngs, R. Graves, and G. Atkinson (2018). Central and Eastern North America ground-motion characterization: NGA-East final report, *PEER Rept. 2018/08*, Pacific Earthquake Engineering Research Center, 817 pp.

Hanks, T. C., and H. Kanamori (1979). A moment magnitude scale, *J. Geophys. Res.* **84**, 2348–2350.

McGuire, R. K., W. J. Silva, and C. J. Costantino (2001). Technical basis for revision of regulatory guidance on design ground motions: Hazard-and risk-consistent ground motion spectra guidelines, *NUREG/CR-6728*, U.S. Nuclear Regulatory Commission, Washington, D.C.

Miller, A. C., and T. R. Rice (1983). Discrete approximations of probability distributions, *Manage. Sci.* **29,** 352–362.

R Core Team (2022). R: A language and environment for statistical computing, R Foundation for Statistical Computing, Vienna, Austria.

Rodriguez-Marek, A., J. Ake, C. Munson, E. Rathje, S. Stovall, T. Weaver, K. Ulmer, and M. Juckett (2021). Documentation report for SSHAC Level 2: Site response, Center for Nuclear Waste Regulatory Analysis, San Antonio, Texas, available at https://www.nrc.gov/docs/ML2132/ML21323A056.pdf (last accessed August 2022).

Rodriguez-Marek, A., J. J. Bommer, R. R. Youngs, M. J. Crespo, P. J. Stafford, and M. Bahrampouri (2021). Capturing epistemic uncertainty in site response, *Earthq. Spectra* **37,** 921–936.

Rodriguez-Marek, A., E. M. Rathje, J. J. Bommer, F. Scherbaum, and P. J. Stafford (2014). Application of single-station sigma and site-response characterization in a probabilistic seismic-hazard analysis for a new nuclear site, *Bull. Seismol. Soc. Am.* **104**, 1601–1619.

Salvatier, J., T. V. Wiecki, and C. Fonnesbeck (2016). Probabilistic programming in Python using PyMC3, *PeerJ. Comput. Sci.* **2,** e55, doi: 10.7717/peerj-cs.55.

Scherbaum, F., F. Cotton, and H. Staedtke (2006). The estimation of minimum-misfit stochastic models from empirical ground-motion prediction equations, *Bull. Seismol. Soc. Am.* **96,** 427–445.

Scherbaum, F., N. M. Kuehn, M. Ohrnberger, and K. Koehler (2010). Exploring the proximity of ground-motion models using high-dimensional visualization techniques, *Earthq. Spectra* **26,** 1117–1138.

Silva, W., B. Darragh, T. Kishida, O.-J. Ktenidou, and E.-V. Pikoulis (2021). INL SSHAC Level 3 study: Estimation of source, path, and site parameters and their uncertainty, *INL Rept. INL/EXT-21-65281*, Idaho National Laboratory, Idaho Falls, Idaho, 259 pp.

Skarlatoudis, A. A., C. B. Papazachos, B. N. Margaris, N. Theodulidis, C Papaioannou, I. Kalogeras, E. M. Scordilis, and V. Karakostas (2003). Empirical peak ground-motion predictive relations for shallow earthquakes in Greece, *Bull. Seismol. Soc. Am.* **93,** 2591–2603.

Spudich, P., and D. M. Boore (2005). *Erratum to*: SEA99: A Revised Ground Motion Prediction Relation for Use in Extensional

Tectonic Regimes, by P. Spudich, W. B. Joyner, A. G. Lindh, D. M. Boore, B. M. Margaris, and J. B. Fletcher, Bull. Seismol. Soc. Am. 89, 1156–1170, *Bull. Seismol. Soc. Am.* **95**, no. 3, 1209.

Spudich, P., J. B. Fletcher, M. Hellweg, J. Boatwright, C. Sullivan, W. B. Joyner, T. C. Hanks, D. M. Boore, A. McGarr, L. M. Baker, *et al.* (1996). Earthquake ground motions in extensional tectonic regimes, *U.S. Geol. Surv. Open-File Rept. 96-292*, 351 pp.

Spudich, P., W. B. Joyner, A. G. Lindh, D. M. Boore, B. M. Margaris, and J. B. Fletcher (1999). SEA99: A revised ground motion prediction relation for use in extensional tectonic regimes, *Bull. Seismol. Soc. Am.* **89,** 1156–1170.

Stafford, P. J., D. M. Boore, R. R. Youngs, and J. J. Bommer (2022). Host-region parameters for an adjustable model for crustal earthquakes to facilitate the implementation of the backbone approach to building ground-motion logic trees in probabilistic seismic hazard analysis, *Earthq. Spectra* **38,** 917–949.

U.S. Nuclear Regulatory Commission (USNRC) (2018). Updated implementation guidelines for SSHAC hazard studies, *NUREG-2213*, U.S. Nuclear Regulatory Commission, Washington, D.C.

Venables, W. N., and B. D. Ripley (2002). *Modern Applied Statistics with S*, Fourth Ed., Springer, New York, New York, 495 pp.

# APPENDIX

## Adjusting the CY14 source scaling for changes in the stress parameter

Bommer and Stafford (2020, top left column of p. 2811) suggested that changes in stress parameters can be accounted for by differences in $c_M$ in the Chiou and Youngs (2014; hereafter, CY14) source scaling; but they gave no details. This section provides those details.

The source scaling $F_S$ in CY14 is given primarily by equation (1c), repeated here for convenience:

$$F_S = c_2(\mathbf{M} - 6) + \frac{c_2 - c_3}{c_n}\ln[1 + e^{c_n(c_M - \mathbf{M})}]. \qquad \text{(A1)}$$

We say "primarily," because there is also **M** dependence of $\ln y_{\text{ref}}$ in the $F_{\text{SoF}}$, $F_{\text{Ztor}}$, $F_{\text{Dip}}$, $F_{\text{GS}}$, and $F_A$ functions. But those functions are not expected to depend on the source scaling as controlled by the stress parameter $\Delta\sigma$. Although it is a continuous, smoothly varying function, the $F_S$ can be thought of as being constructed from two essentially linear segments joined by a short transition segment (an example is shown in Fig. 7). The intersection of the two linear segments occurs at $\mathbf{M} = c_M$. We refer to the essentially linear segments as segment 1, for which the **M** scaling is determined by the source function at frequencies less than the source corner frequency, and is therefore independent of the stress parameter, and segment 2, whose magnitude scaling is influenced by the stress parameter. Because of the relation of the magnitude scaling to the source spectra, the slope of segment 1 is greater than that of segment 2.

To understand how to change the CY14 source scaling to account for differences in $\Delta\sigma$, it is useful to consider a plot of the Fourier acceleration spectra (FS) from a single corner frequency, constant stress parameter source for a suite of moment magnitudes **M**. Such a plot is shown in Figure A1a for $R_{\text{JB}} = 10$ km, **M** ranging from 4 to 8 in increments of 0.5, and $\Delta\sigma = 100$ bars. To see the scaling of FS with **M**, we plotted FS versus **M** in Figure A1b for a frequency of 0.5 Hz (this frequency is shown by the vertical line in Figure A1a). The straight lines in Figure A1b were obtained by fitting lines to the small and large **M** portions of the FS. The magnitude scaling for FS is similar to that for response spectra (RS) for the CY14 ground-motion prediction model (GMPM) (e.g., Fig. 7) with line segments for small and large **M** intersecting at a hinge magnitude. (For the sake of brevity in the notation, we use FS for Fourier amplitude spectra (FAS) and RS for pseudo-acceleration response spectra (PSA) in this appendix, rather than FAS and PSA as in the main body of the article.) Because of the similarity to the CY14 magnitude scaling, we call the hinge magnitude $c_M$. The following analysis first derives a relation based on a model of the scaling of FS, giving the change in $c_M$ due to changing the stress parameter from $\Delta\sigma_1$ to $\Delta\sigma_2$. An adjustment is then derived to account for differences in the magnitude-scaling slopes of FS and RS. We added FS and RS as subscripts to $c_M$ to differentiate between the hinge magnitudes for FS and RS, when necessary. For simplicity of notation, however, we did not add an additional subscript to $c_M$ in most of the first section, which deals only with FS.

## Changes in the hinge magnitude for Fourier spectra due to changes in the stress parameter

To see the effect of a change in $\Delta\sigma$, the FS for $\Delta\sigma = 50$ bars has been added to Figure A1a, with the result shown in Figure A1c. There are two things to note in this figure that need to be captured in modifications of the CY14 equation to account for a different stress parameter: (1) the curves are independent of $\Delta\sigma$ for frequencies less than the source corner frequencies, and (2) the source corner frequencies vary with $\Delta\sigma$ (such that the high-frequency FS is reduced if $\Delta\sigma$ is reduced and vice versa).

The source scaling for $\Delta\sigma = 50$ bars has been added to Figure A1b, resulting in Figure A1d. The results in the figure show that changes in $\Delta\sigma$ can be captured by changing $c_M$ in equation (A1) to $c_M + \Delta c_M$, so that equation (A1) becomes

$$F_S = c_2(\mathbf{M} - 6) + \frac{c_2 - c_3}{c_n}\ln[1 + e^{c_n(c_M + \Delta c_M - \mathbf{M})}]. \qquad \text{(A2)}$$

Although this equation accounts for the stress parameter dependence of FS for large magnitudes, it also includes a stress-parameter dependence of the motion for small magnitudes. This can be seen by taking the asymptotic limit of equation (A2) for $M \ll c_M - \Delta c_M$. Because the CY14 coefficients give $c_n c_M > 10$ for all periods, and $\Delta c_M$ is expected to be relatively small (e.g., −0.2 in Figure A1d), the asymptotic limit of equation (A2) for small **M** becomes

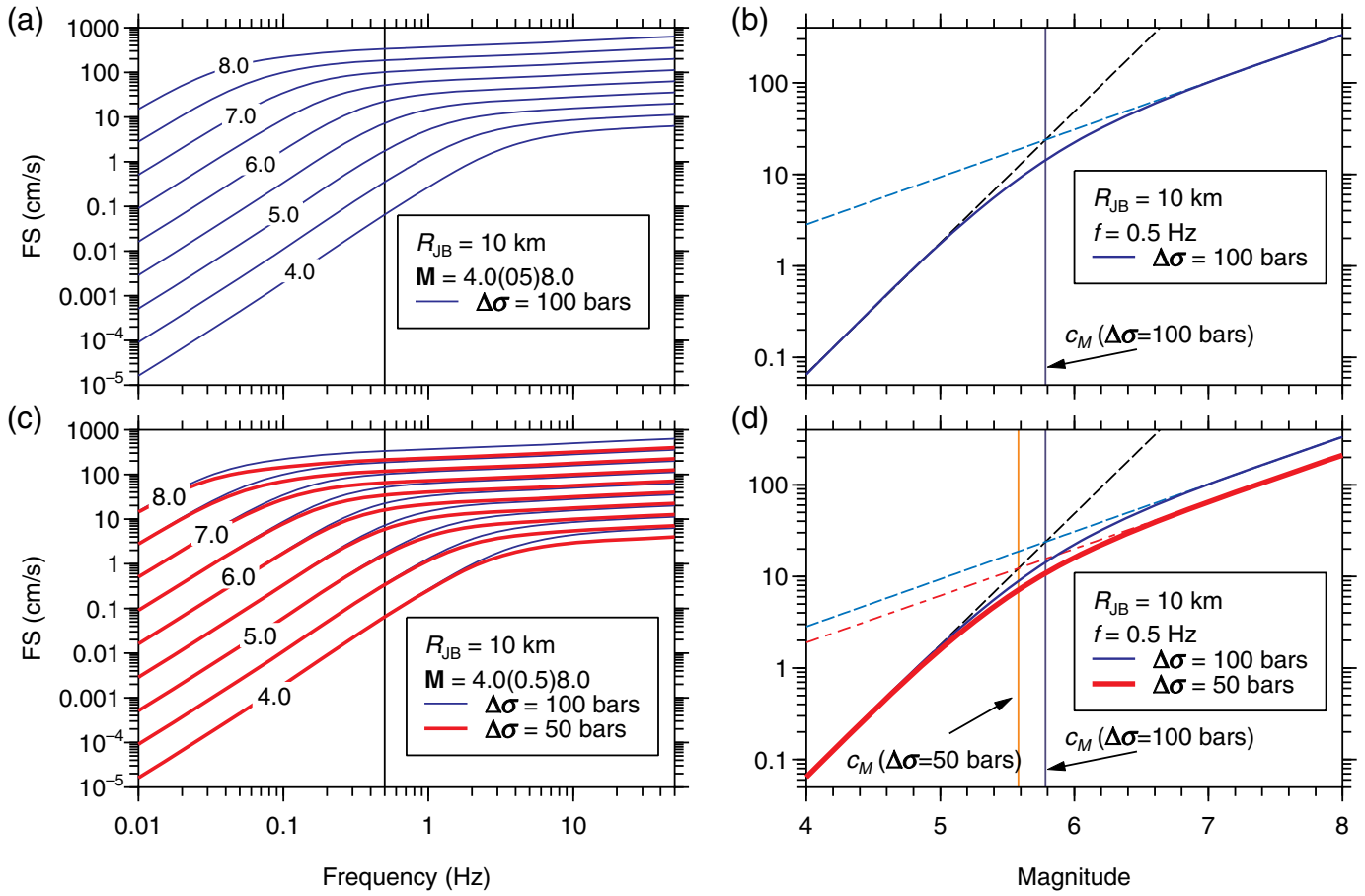


**Figure A1.** Illustration of the dependence of the magnitude scaling on the stress parameter $\Delta\sigma$ (a detailed description of panels (a–d) is given in the text of this Appendix). As a side note, the Fourier spectra (FS) in (a) and (c) rises slowly at high frequencies rather than being flat, as implied by equation (A5), because the Al Atik and Abrahamson (2021) crustal amplifications, which increase with frequency, have been included (and $\kappa_0 = 0$ s, so the FS at high frequencies is not reduced). The color version of this figure is available only in the electronic edition.

$$F_S \rightarrow c_2(\mathbf{M}-6) + (c_2-c_3)(c_M-\mathbf{M}) + (c_2-c_3)\Delta c_M. \quad \text{(A3)}$$

This shows that the last term in equation (A3) needs to be subtracted from equation (A2) to remove the stress-parameter dependence of $F_S$ for small **M**. Doing this gives the proper equation for accounting for $\Delta\sigma$ differences by changing $c_M$, as given in equation (A4):

$$F_S = c_2(\mathbf{M}-6) + \frac{c_2-c_3}{c_n}\ln[1+e^{c_n(c_M+\Delta c_M-\mathbf{M})}] - (c_2-c_3)\Delta c_M. \quad \text{(A4)}$$

Because applications of equation (A4) will generally involve determinations of $\Delta\sigma$ in host and target regions, the remaining parts of the analysis (1) develop an explicit relation between $\Delta c_M$ and different $\Delta\sigma$ and then (2) derive adjustments needed to account for the different magnitude scaling of FS and RS.

Let $\Delta\sigma_1$ and $\Delta\sigma_2$ be the stress parameters in the host and target regions, respectively. The equation for the single corner frequency source spectrum $E$ is

$$E(f) = \frac{CM_0 f^2}{1+\left(\frac{f}{f_c}\right)^2}, \quad \text{(A5)}$$

in which $C$ is a constant, $M_0$ is seismic moment, and the corner frequency $f_c$ is given by

$$f_c = \xi\left(\frac{\Delta\sigma}{M_0}\right)^{\frac{1}{3}}, \quad \text{(A6)}$$

in which $\xi$ is a constant ($4.906\times10^6\beta_s$, when the units of $f_c$, $\Delta\sigma$, $M_0$, and $\beta_s$ [the shear-wave velocity in the vicinity of the source] are Hz, bars, dyn · cm, and km/s, respectively). The seismic moment $M_0$ is related to the moment magnitude using the following equation (from Hanks and Kanamori, 1979):

$$\log M_0 = 1.5\mathbf{M} + 16.05. \quad \text{(A7)}$$

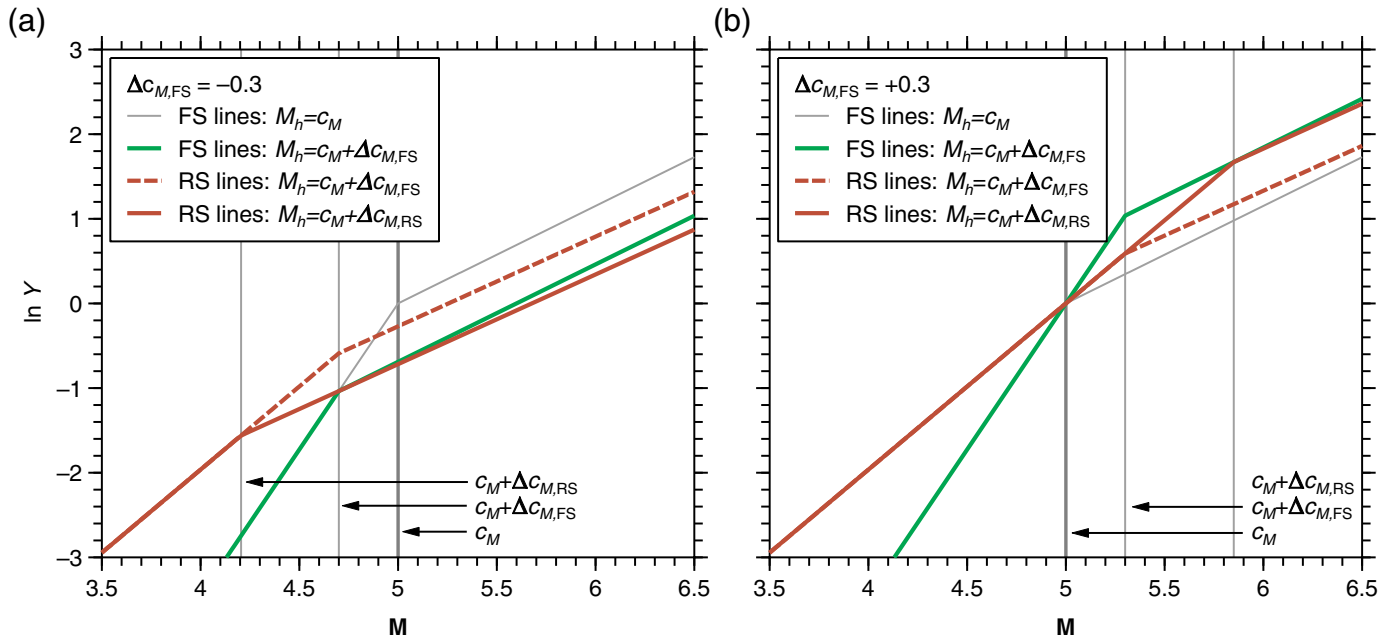


**Figure A2.** Illustrating the scaling of FS and response spectra (RS) for (a) negative and (b) positive shifts in $\Delta c_{M,FS}$, showing that the shift in $\Delta c_{M,RS}$ needs to be modified from that for $\Delta c_{M,FS}$ in order for the RS amplitude of line-segment 2 to be similar to that of the FS line-segment 2 amplitude. The color version of this figure is available only in the electronic edition.

Following the graphical presentation, lines are to be fit to $\log E$ versus **M** for the low and high portions of **M**, at fixed frequency $f$. The logarithm of equation (A5) is

$$\log E = \log CM_0 f^2 - \log\left[1 + \left(\frac{f}{\xi}\right)^2 \left(\frac{M_0}{\Delta\sigma}\right)^{\frac{2}{3}}\right]. \quad \text{(A8)}$$

The low- and high-magnitude asymptotes of $\log E$ are straight lines in terms of $\log(M_0)$, as given by these equations:

Small $M_0$:

$$\log E = \log CM_0 f^2, \quad \text{(A9)}$$

Large $M_0$:

$$\log E = \log CM_0 f^2 - 2\log\left(\frac{f}{\xi}\right) - \frac{2}{3}\log M_0 + \frac{2}{3}\log\Delta\sigma. \quad \text{(A10)}$$

The hinge magnitude ($c_M$) is the intersection of the two lines; it is determined by equating equations (A9) and (A10), converting $M_0$ to **M** using equation (A7), and solving for $c_M$. This results in equation (A11):

$$c_M = \frac{2}{3}\log\Delta\sigma - \frac{2}{3}16.05 - 2\log\frac{f}{\xi}. \quad \text{(A11)}$$

The difference in $c_M$ for two values of $\Delta\sigma$ then becomes

$$\Delta c_{M,FS} = \frac{2}{3}\log\frac{\Delta\sigma_2}{\Delta\sigma_1}. \quad \text{(A12)}$$

We added "FS" to the subscript of $\Delta c$ to indicate that the equation applies to the scaling of Fourier spectra (FS) not RS. For the graphical example:

$$\Delta c_{M,FS} = c_{M2} - c_{M1} = \frac{2}{3}\log\frac{50}{100} = -0.20, \quad \text{(A13)}$$

which is the same difference seen in Figure A1d (within round-off).

## Modifying the hinge magnitude for use with RS

A modification to equation (A12) is needed the account for differences in the slopes of line segments 1 and 2 for FS and for RS. As shown in Table A1 (in which, for convenience, we use notation $s_{1,FS}$, $s_{1,RS}$, $s_{2,FS}$, and $s_{2,RS}$ to indicate the slopes of line segments 1 and 2, for FS and for RS), the RS slopes are always less than the FS slopes for all periods. The consequence of using $\Delta c_{M,FS}$ with the RS slopes is shown by the dashed lines in Figure A2 for negative and positive changes in $c_M$. That figure is a schematic representation of the magnitude scaling of the logarithm of a ground-motion intensity measure ($\ln Y$). Because we are only interested in differences in ln FS and ln RS, we assume in Figure A2 that the segment 1 and 2 lines for FS and RS corresponding to the stress parameter $\Delta\sigma_1$ (the host region) have values of 0.0 at **M** 5.0. The slopes of the RS line segments in Figure A2 correspond to the CY14 coefficients

TABLE A1
**Slopes of Line Segments and $\chi_{FS2RS}$ Adjustments**

| | | | | | $\chi_{FS2RS}$ | |
|---|---|---|---|---|---|---|
| **T (s)** | **$s_{1,FS}$** | **$s_{1,RS}$** | **$s_{2,FS}$** | **$s_{2,RS}$** | **$\Delta c_{M,FS} < 0$** | **$\Delta c_{M,FS} > 0$** |
| 0.010 | 3.454 | 1.964 | 1.151 | 1.060 | 2.649 | 2.835 |
| 0.020 | 3.454 | 1.964 | 1.151 | 1.060 | 2.649 | 2.835 |
| 0.030 | 3.454 | 1.964 | 1.151 | 1.060 | 2.649 | 2.835 |
| 0.040 | 3.454 | 1.964 | 1.151 | 1.060 | 2.649 | 2.835 |
| 0.050 | 3.454 | 1.964 | 1.151 | 1.060 | 2.649 | 2.835 |
| 0.075 | 3.454 | 1.964 | 1.151 | 1.060 | 2.649 | 2.835 |
| 0.100 | 3.454 | 1.964 | 1.151 | 1.060 | 2.649 | 2.835 |
| 0.150 | 3.454 | 2.036 | 1.151 | 1.060 | 2.452 | 2.602 |
| 0.200 | 3.454 | 2.152 | 1.151 | 1.060 | 2.192 | 2.301 |
| 0.300 | 3.454 | 2.344 | 1.151 | 1.060 | 1.864 | 1.931 |
| 0.400 | 3.454 | 2.471 | 1.151 | 1.060 | 1.697 | 1.745 |
| 0.500 | 3.454 | 2.557 | 1.151 | 1.060 | 1.599 | 1.638 |
| 0.750 | 3.454 | 2.681 | 1.151 | 1.060 | 1.477 | 1.505 |
| 1.000 | 3.454 | 2.747 | 1.151 | 1.060 | 1.419 | 1.443 |
| 1.500 | 3.454 | 2.816 | 1.151 | 1.060 | 1.363 | 1.383 |
| 2.000 | 3.454 | 2.851 | 1.151 | 1.060 | 1.336 | 1.354 |
| 3.000 | 3.454 | 2.888 | 1.151 | 1.060 | 1.310 | 1.326 |
| 5.000 | 3.454 | 2.917 | 1.151 | 1.060 | 1.289 | 1.304 |
| 7.500 | 3.454 | 2.932 | 1.151 | 1.060 | 1.279 | 1.293 |
| 10.000 | 3.454 | 2.940 | 1.151 | 1.060 | 1.274 | 1.288 |

For a single corner frequency, constant stress parameter source model, $s_{1,FS} = 1.5 \ln 10 = 3.454$ and $s_{2,FS} = 0.5 \ln 10 = 1.151$. $s_{1,RS}$ and $s_{2,RS}$ are the CY14 coefficients $c_3$ and $c_2$, respectively.

for $T = 0.1$ s, but the $\Delta c_{M,FS}$ of $\pm 0.3$ was chosen for the sake of illustrating the discussion here (the actual values of $\Delta c_{M,FS}$ range from −0.15 to +0.06). It is clear from the dashed lines in Figure A2 that using $\Delta c_{M,FS}$ as an adjustment to $c_M$ results in values of ln RS that are very different than ln FS for line segment 2. We want to determine a shift $\Delta c_{M,RS}$ such that the change in ln RS is the same as the change in ln FS produced by changing the stress parameter from $\Delta\sigma_1$ to $\Delta\sigma_2$. Because the slopes $s_{2,FS}$ and $s_{2,RS}$ are not equal, the change in ln FS and ln RS will not be the same for all magnitudes. Our choice for $\Delta c_{M,FS} > 0$ is to find $\Delta c_{M,RS}$ such that the line with the slope $s_{1,RS}$ intersects line segment 2 of the ln FS function corresponding to $\Delta\sigma_2$. For $\Delta c_{M,FS} < 0$, we choose $\Delta c_{M,RS}$ such that line segment 2 for ln RS intersects line segment 2 of the ln FS function at $c_M + \Delta c_{M,FS}$ (see Fig. A2).

For $\Delta c_{M,FS} > 0$, the change in ln RS produced by a shift in the hinge magnitude from $c_M$ to $c_M + \Delta c_{M,RS}$ is

$$\Delta \ln \mathrm{RS} = s_{1,RS} \Delta c_{M,RS}, \tag{A14}$$

and the change in ln FS for the same shift in the hinge magnitude is given by

$$\Delta \ln \mathrm{FS} = s_{1,FS} \Delta c_{M,FS} + s_{2,FS} (\Delta c_{M,RS} - \Delta c_{M,FS}). \tag{A15}$$

Equating equations (A14) and (A15) gives the following equation for $\Delta c_{M,RS}$:

$$\Delta c_{M,RS} = \chi_{FS2RS} \Delta c_{M,FS}, \tag{A16}$$

in which

$$\chi_{FS2RS} = \frac{s_{1,FS} - s_{2,FS}}{s_{1,RS} - s_{2,FS}}, \quad \text{for } \Delta c_{M,FS} > 0. \tag{A17}$$

A similar analysis for $\Delta c_{M,FS} < 0$ finds the same equation for $\Delta c_{M,RS}$ (equation A16) but with

$$\chi_{FS2RS} = \frac{s_{1,FS} - s_{2,RS}}{s_{1,RS} - s_{2,RS}}, \quad \text{for } \Delta c_{M,FS} < 0. \tag{A18}$$

The adjustment to the source function $F_S$ for a host-region $\Delta\sigma_1$ and a target-region $\Delta\sigma_2$ is thus given by equation (A4) with

$$\Delta c_M = \chi_{FS2RS} \frac{2}{3} \log \frac{\Delta\sigma_2}{\Delta\sigma_1}, \tag{A19}$$

in which $\chi_{FS2RS}$ is given either by equation (A17) or (A18), depending on the sign of $\Delta c_{M,FS}$ (equation A12).

The revised ln $Y$ corresponding to a change in the stress parameters is now shown by the solid RS lines in Figure A2. Table A1 gives $\chi_{FS2RS}$ for the CY14 GMPM.

**Manuscript received 8 April 2022**
**Published online 30 August 2022**